

# **Extraction of Natural Dyes for Economical and Efficient Fabrication of Dye Sensitized Solar Cells**

**M. Tech. Thesis**

By  
**Akula Surya Teja**



**DEPARTMENT OF METALLURGICAL ENGINEERING AND  
MATERIALS SCIENCE  
INDIAN INSTITUTE OF TECHNOLOGY INDORE  
May 2023**

# **Extraction of Natural Dyes for Economical and Efficient Fabrication of Dye Sensitized Solar Cells**

**A THESIS**

*Submitted in partial fulfillment of the  
Requirements for the award of the degree  
of  
Master of Technology*

*by*  
**Akula Surya Teja**



**DEPARTMENT OF METALLURGICAL  
ENGINEERING AND MATERIALS SCIENCE  
INDIAN INSTITUTE OF TECHNOLOGY INDORE  
May 2023**



# INDIAN INSTITUTE OF TECHNOLOGY INDORE

## CANDIDATE'S DECLARATION

I certify that the research work provided in this thesis, which has a title **Extraction of Natural Dyes for Economical and Efficient Fabrication of Dye Sensitized Solar Cells** in the partial fulfilment of the criteria for granting the degree of **MASTER OF TECHNOLOGY** and submitted in the **DEPARTMENT OF METALLURGICAL ENGINEERING AND MATERIALS SCIENCE, INDIAN INSTITUTE OF TECHNOLOGY INDORE**, is a true representation of the work I did for myself between the dates from 09 Aug of joining the II year M.Tech. program to June 2023 of M.Tech. Thesis submission under the supervision of Dr.Parasharam M.Shirage, Professor, Department of MEMS.

The matter articulated within this thesis has not been previously presented by myself as a requirement for obtaining any other academic degree, either from this institution or any other accredited academic institution.

*A. Akula*  
5/6/23

Signature of the student with date  
Akula Surya Teja

-----  
This is to certify that the statement above made by the candidate is genuine to the best of my/our knowledge.

*Dr. Parasharam M. Shirage*  
5/6/2023

Signature of the Supervisor of  
M.Tech. thesis #1 (with date)

Prof. PARASHARAM M. SHIRAGE

**Dr. Parasharam M. Shirage**  
**Professor**  
**Department of Metallurgy Engineering**  
**and Materials Science (MEMS)**  
**Indian Institute of Technology Indore**  
**Khandwa Road, Simrol,**  
**INDORE-453552 INDIA**

-----  
**Akula Surya Teja** has successfully given his M.Tech. Oral Examination held on **25/05/2023**.

Signature(s) of Supervisor(s) of M.Tech. thesis

Date: 5/6/2023

Signature of PSPC Member #1

Date:

*Kiran Bala*  
5/6/2023  
**Dr. Kiran Bala**

Convener, DPGC

Date:

*Santosh Hosmani*  
5/6/2023  
Signature of PSPC Member #2

Date:

**Dr. Santosh Hosmani**



## ACKNOWLEDGEMENTS

Firstly, I want to start by genuinely thanking my thesis advisor **Prof. Parasharam M. Shirage** for his unwavering guidance of my M.Tech. Project and associated research, as well as for his patience, encouragement, and vast expertise. I want to acknowledge and express and sincerely thank our Director **Prof. Suhas S. Joshi** for providing me with the necessary resources and letting me to work in a pleasant atmosphere. I would like to take this chance to thank my PSPC members **Dr. Santosh Hosmani** and **Dr. Kiran Bala** for their insightful suggestions.

I am especially thankful for the support given by Mr. Subhash Chand Yadav for his helpful and effective suggestions in the course of the planning and evolution of this research work. Also, I would want to thank Mr. Abhishek Srivastava for being so willing to assist me out with everything and for giving his time so generously. I also want to express my sincere thanks to everyone in my AFMRG lab. I'm grateful to every member in the AFMRG lab for their never-ending motivation and enjoyable conversations.

Lastly, I would like to acknowledge my parents for their unwavering encouragement and motivation all through my years of study, as well as during the process of gathering information for and writing this thesis.

## **DEDICATION**

*Dedicated to my Parents, friends,  
And teacher*

## **ABSTRACT**

The third generation of solar cells are dye-sensitized solar cells, or DSSCs. It falls under the broader category of thin-film solar cells. With the help of electrolytes or solid charge-transporting materials, dye-sensitized solar cells (DSSCs) transform sunlight into energy by utilising photosensitizers that are adsorbed onto the surface of nanocrystalline mesoporous titanium dioxide ( $\text{TiO}_2$ ) films. They have received a lot of research attention for over two decades because of their affordable price, simple manufacturing, low toxicity, and scalability. If efficient forms of energy can be produced for usage in prevailing inside circumstances, photovoltaic (PV) technologies have the potential to turn our buildings "independent" plus our movable gadgets "smart." In this study,  $\text{TiO}_2$  nanorods (TNRs) are synthesised, and their structural, morphological, optical, and photo-electrochemical characteristics are examined, along with their potential applicability in dye-sensitized solar cells (DSSCs). Several studies were focused on reducing the cost of present DSSCs and enhancing their flexibility by using adaptable materials that could cut the cost of this energy conversion technique and expand their uses. In this study, Spinacia Oleracea Leaves (SOL), and Ixora Coccinea Flower (ICF) extracts were utilised as sensitizers for DSSCs application. From the extracted dyes, it was observed that SOL has significant amount of Chlorophyll pigments while IOF was dominated by Anthocyanin pigments. The produced TNRs and natural dyes were subjected to various physicochemical characterizations using FESEM, XRD, UV-Vis spectroscopy, FTIR, Raman spectroscopy, etc. The photovoltaic investigations evaluated the co-sensitized dyes' significantly improved visible-light photo electrochemical performance. Employing electrochemical impedance spectroscopy (EIS), the interfaces between natural dyes and TNR layers had been examined. This study also examines

the functions of various inexpensive and environmentally friendly counter electrodes. Employing co-sensitization method, we fabricated dye-sensitized solar cells. These cells use TiO<sub>2</sub> nanorods as the working electrode, carbon and nickel-based counter electrodes, *Ixora coccinea* and *Spinacia oleracea* as dyes, and an iodine-based electrolyte to produce electricity under ambient light conditions. These solar cells have displayed an exceptional conversion efficiency of 2.39%. In comparison to the single natural SOL and ICF-dyes based DSSC, the optimal co-sensitized DSSC demonstrated 2.3- and 4.2-times improved efficiency, accordingly. This improvement in performance is considered a co-dominant effect.

**Key words:** Dye sensitized solar cell, TiO<sub>2</sub> Nano rods, hydrothermal process, *Ixora Coccinea*, *Spinacia Oleracea*, Potassium Iodide, Iodine crystal

## List of Publications

First Author:

1. **Teja, Akula Surya**, Abhishek Srivastava, Jena Akash Kumar Sathrughna, Manish Kumar Tiwari, Archana Kanwade, Subhash Chand Yadav, and Parasharam M. Shirage. "Optimal processing methodology for futuristic natural dye sensitized solar cells and novel applications." *Dyes and Pigments* (2022): 110997. **(Impact factor:5.122)**
2. **Akula Surya Teja**,<sup>a,#</sup> Abhishek Srivastava,<sup>a,#</sup> Jena Akash Kumar Satrughna,<sup>b</sup> Manish Kumar Tiwari,<sup>a</sup> Archana Kanwade,<sup>a</sup> Hyunju Lee,<sup>c</sup> Atsushi Ogura,<sup>c</sup> Parasharam M. Shirage. "Synergistic Co-Sensitization of Environment-Friendly Chlorophyll and Anthocyanin-based Natural Dye-Sensitized Solar Cells: An Effective Approach towards Enhanced Efficiency and Stability". *Solar Energy*(2023): (Under Review) **(Impact factor:7.188)**

Co-Author:

1. Satrughna, Jena Akash Kumar, Archana Kanwade, Abhishek Srivastava, Manish Kumar Tiwari, Subhash Chand Yadav, **Surya Teja Akula**, and Parasharam M. Shirage. "Experimental and ab

initio based DFT calculation of  $\text{NaFe}_{0.5}\text{Co}_{0.5}\text{O}_2$  as an excellent cathode material for futuristic sodium ion batteries." *Journal of Energy Storage* 65 (2023): 107371.(Impact factor:8.907)

## Table of Contents

ACKNOWLEDGEMENTS.....	v
ABSTRACT .....	vi
List of Figure .....	xiii
Chapter 1 .....	1
1. Introduction .....	1
1.1. Solar cell .....	1
1.2. Solar cell types .....	5
1.3. Dye sensitized solar cell.....	8
1.4. DSSC Structure and Working concept; .....	9
1.6 Thesis structure.....	14
Chapter 2.....	15
2. Analysis of Previous Research Work and approach to Problem.....	15
2.2. Work motive: .....	20
Chapter 3.....	22
Experimenting Techniques .....	23
3.1 Experimenting Techniques: .....	23
3.1.1. Process of Spin coating .....	23
3.1.2. Hydrothermal Synthesis method .....	24
3.2. Synthesis and design of dye-sensitized solar cell .....	25
3.2.2. FTO glass substrate cleansing .....	26
3.2.3. Fabrication of compact (c) TiO <sub>2</sub> layer and TiO <sub>2</sub> Nanorods .....	27
3.2.4. Preparation of Cocktail of Natural dyes .....	28
3.2.5. Preparation of Electrolyte .....	29
3.2.6. Synthesis of Counter Electrode .....	30
3.3 Various analytical and Characterization Techniques.....	30

3.3.1. Calculation of Fill Factor and Efficiency employing Current density – Voltage (J-V) curves.....	30
3.3.2) X-ray diffraction (XRD) .....	31
3.3.3 Scanning Electron Microscope (SEM).....	34
3.3.4 UV-Visible spectroscopy .....	35
Chapter 4 .....	37
Results and Discussion .....	37
4.1 Investigation of TiO <sub>2</sub> layer.....	37
4.1.1 XRD analyses of TiO <sub>2</sub> layer.....	37
4.1.2 FE-SEM Analyses of TiO <sub>2</sub> Nanorods.....	39
4.1.3 UV-Vis spectroscopy analyses of TiO <sub>2</sub> Nanorods.....	40
4.1.4 Raman spectroscopy .....	42
Conclusions and Future Potential .....	47
References .....	49

## List of Figure

Figure 1.1 solar energy produced by the nuclear fusion process .....	1
Figure 1.2 Cumulative solar pv capacity .....	2
Figure 1.3 The semiconductor p-n junction solar cell under load.....	<b>Error!</b>
<b>Bookmark not defined.</b>	
Figure 1.4 Current development patterns and various kinds of Solar cell Technologies.....	5
Figure 1.5 (a) Mono-crystalline Si solar cell (b) Poly-crystalline Si solar cell. ....	8
Figure 1.6 Efficiency versus price per watt for three different generations' solar cell .....	10
Figure 1.7 Schematic working mechanism illustration of the DSSC.....	13
Figure 1.8 J-V Characteristic curve of DSSC.....	16
Figure 2.1 Schematic representation for fabrication of DSSC.....	17
Figure 3.1 Stages of spin coating technique on substrate.....	24
Figure 3.2 a) Teflon liner, and b) Stainless steel Autoclave.....	25
Figure 3.3 TiO <sub>2</sub> coated FTO substrate after hydrothermal synthesis .....	30
Figure 3.4 Schematics of solar simulator .....	34
Figure 3.5 Schematic of X-ray diffraction .....	35
Figure 3.6 Fundamental parts of a X-ray diffractometer .....	36
Figure 3.7 Basic construction of a SEM .....	38
Figure 3.8 The experimental set-up of UV-Vis spectrometer .....	36
Figure 4.1 XRD pattern and peaks of TiO <sub>2</sub> NR photoanodes on c-TiO <sub>2</sub> coated FTO substrate. ....	41
Figure 4.2. Typical surface morphology and composition analysis FESEM images .....	43
Figure 4.2.1 Uniformly vertically aligned TiO <sub>2</sub> NRs grown over the FTO substrate by hydrothermal method. ....	43
Figure 4.3 UV-Visible spectroscopy analysis. ....	44
Figure 4.3 (a) Absorption spectra of hydrothermally synthesized TNRs. ...	44
Figure 4.3 (b) Bandgap estimation of the TNRs .....	44

Figure 4.3 (c) Absorption spectra of the SOL(red),ICF(black), and cocktail(green) dyes.....44

Figure 4.4. Raman spectra of the hydrothermally synthesized TNRs on the c-TiO<sub>2</sub> coated FTO substrates. ....**Error! Bookmark not defined.**

Figure 4.5 Photovoltaic analysis of the prepared DSSCs using SOL,ICF, and cocktail dyes.....**Error! Bookmark not defined.**

## ABBREVIATIONS

DI	De-ionized
DMF	Dimethyl formamide
DMSO	Dimethyl sulfoxide
DSSCs	Dye-sensitized solar cells
ETL	Electron transport layer
ETM	Electron transport material
FTO	Fluorine-doped tin oxide
FESEM	Field emission scanning electron microscopy
ITO	Indium-doped tin oxide
HTL	Hole transport layer
HTM	Hole transport material
HOMO	Highest occupied molecular orbital
ICF	Ixora Coccinea Flower
LUMO	Lowest unoccupied molecular orbital
NRs	Nano rods
MAI	Methyl ammonium iodide
MBI	Methyl ammonium bismuth iodide
PCE	Power conversion efficiency
PSCs	Perovskite solar cells
PV	Photovoltaic
SOL	Spinacia Oleracea
TCOs	Transparent conducting oxides

TNRs

Titanium Nanorods

XRD

X-ray diffraction

UV -Vis

Ultra violet- visible



# Chapter 1

## 1. Introduction

### 1.1. Solar cell

Solar energy is generally referred to the immense quantity of energy that the sun produces every day in the form of heat and radiation. It is a cost-free, infinitely renewable source of energy. Solar energy's primary advantage among another conventional power sources is that it could be generated entirely from sunlight by using mini photovoltaic (PV) solar cells. It is believed that the sun is a massive, hot glowing ball of gaseous helium and hydrogen atoms. The release of energy from the nuclear fusion of the hydrogen nuclei in the sun's interior core is what causes this sphere-like, large gaseous cloud, which is primarily made up of multiple hydrogen nuclei, fuse to produce helium energy. (Figure 1.1) [1].

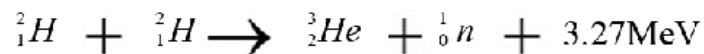
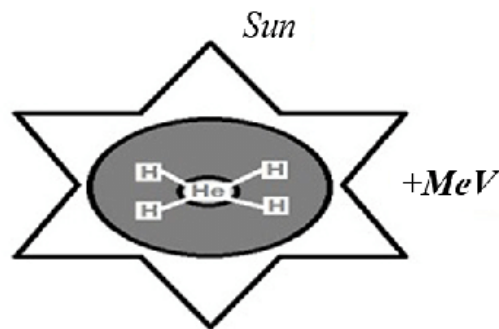
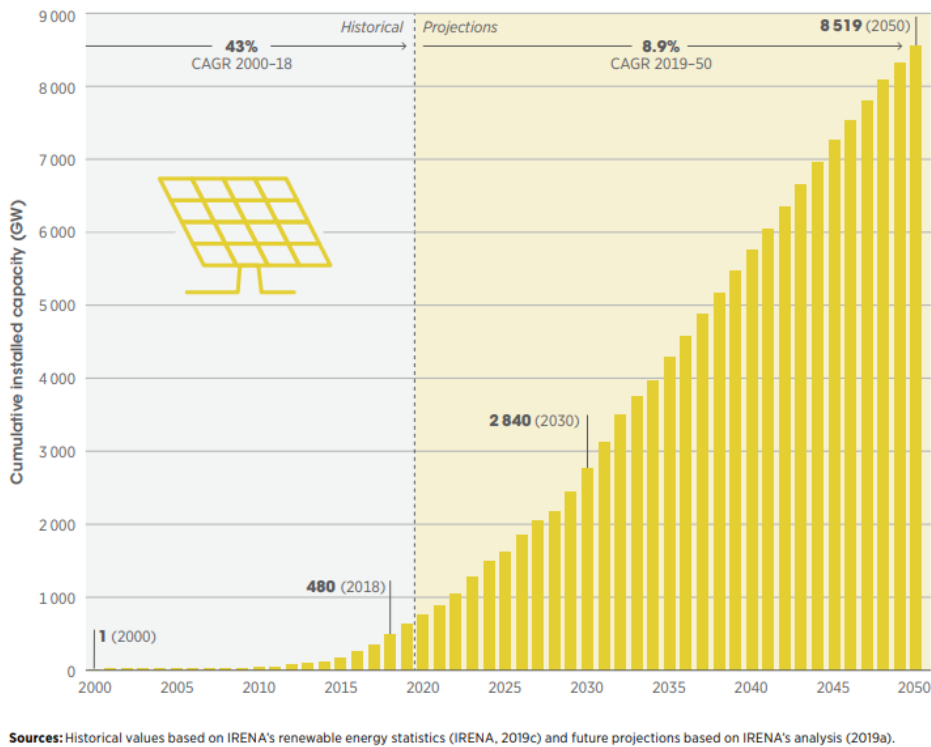


Figure 1.1 Solar energy produced by the nuclear fusion process[1]

Due to the growing concerns about global warming, the health implications on environmental pollution, energy security as well as availability of energy, the volatility of the prices of oil in recent decades, have prompted the demand for alternative, low-carbon technology options like renewable sources. Over the decades, solar photovoltaics (PV) is one among the leading renewable energy technologies. In terms of installed capacity, solar PV was expected to have 480 GW by the end of 2018 (excluding CSP), making it the next-biggest renewable energy source following wind. In the preceding year, solar photovoltaic (PV) installations achieved an impressive record of nearly 94 GW, surpassing all other renewable and power generation capacity additions. Solar PV generated over twice as much energy as wind power and more than the total energy output of nuclear power and fossil fuels consolidated (IRENA, 2019c). The solar PV sector has come a long way, with significant developments recently with respect to installations, costs, and technology, and the development of important associations for solar energy (Figure 1.2). It is evident that solar energy will continue to be a critical renewable energy option in the forthcoming decades.[2]



**Fig 1.2** Cumulative Solar PV capacity [2].

In 2021, the proportion of photovoltaic systems with integrated capacities for commercial and industrial systems will also rise, as they become more profitable in light of rising electricity prices and the nation's electricity shortages [3]. A solar cell, commonly referred to as photovoltaic cell, is a device that uses the photovoltaic effect to transform luminous energy into electricity. Its electrical properties like voltage, current, or resistance, change on exposure to light. which consists primarily of p-n junction diodes. The device produces voltage when light strikes it. It is not new for sunlight to be converted into electricity through the generation of voltage and current when it strikes semiconductors. Since Edmond Becquerel discovered in 1839 the effect of illuminating silver chloride inside an acidic solution, there has been a significant deal of work done to increase the efficiency of such a device, with Bell Labs creating a more efficient version in 1954 [4].

The photovoltaic (PV) effect had been initially studied by Alexandre-Edmond Becquerel in 1839. The photovoltaic effect is a process that produces voltage or electric current in a photovoltaic cell whenever it is illuminated by the sun. It is this effect that makes solar panels functional, because of this, the solar panel's convert sunlight into electrical energy. Following that Russell Ohl designed the first silicon-based modern solar cell in 1946. [5]. Thin silicon wafers used in previous photovoltaic solar cells convert sunlight energy into electrical energy. Figure 1.3 shows how each cell made of two distinct layers (p-type and n-type materials) of a semiconductor material forms an electron hole, which forms the basis of modern photovoltaic technology. In this configuration, an electron is released from the hitting photon by gaining energy and travels from one layer to the other if a photon with enough energy strikes on the p-type and n-type junction. An electron and a hole are created during the process as an outcome, there is a generation of electrical power. For photovoltaic solar cells, a number of materials

are employed, with silicon (single crystal, multi-crystalline, and amorphous silicon), cadmium telluride, copper-indium-gallium-selenide, and copper-indium-gallium-sulfide [6]. The photovoltaic solar cells are divided into numerous classes based on these materials, as explained in the subsequent sections (also depicted in Figure 1.3)

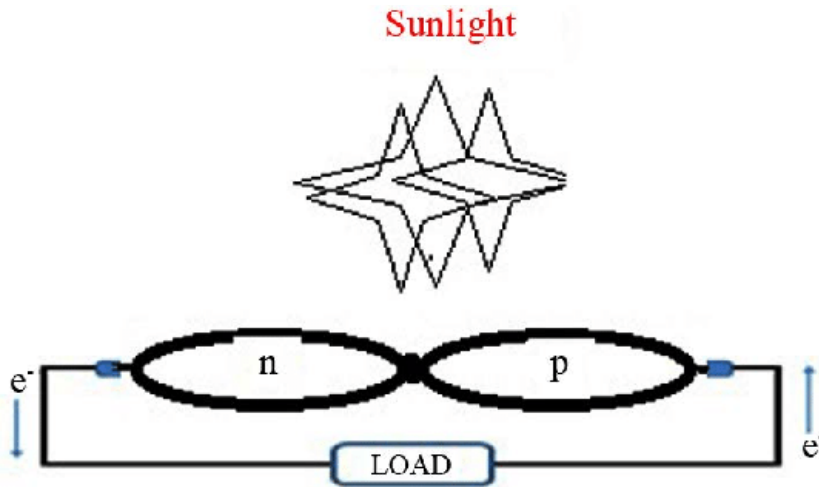


**Fig 1.3** The semiconductor p-n junction solar cell under load [6].

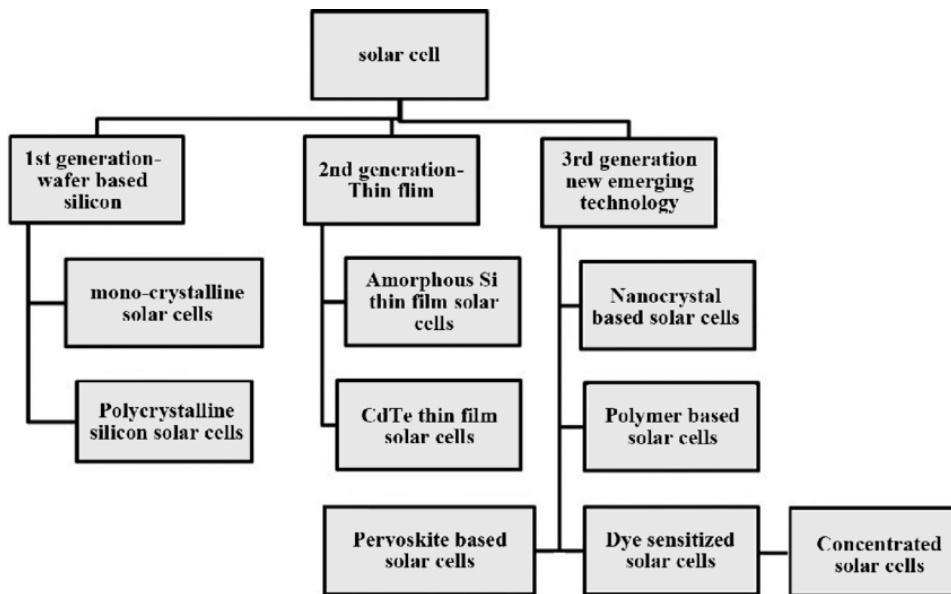


**Figure 1.4** Current development patterns and various kinds of solar cell technologies [6].

The exploration of inexpensive, unlimited energy sources has led to the investigation of renewable energy sources.1–4 During the last thirty years, a lot of research has been concentrated on creating photovoltaic solar cells that are more economical. Dye-sensitized solar cells (DSSC) are amongst eminently efficient photovoltaic devices of the third generation. Because it provides better conversion efficiency in terms of simple production and a low material cost, it might be viewed as an economically efficient alternative for other generations.[7] The recent advancements in technology have significantly improved its potential to address the today's as well as tomorrow's energy requirements. The DSSC is a revolutionary method that employs broad band gap semiconductor sensitization to transform luminous energy to electricity. Over the following years, the study of DSSC gained popularity and researchers found interest in both commercial and fundamental elements of solar energy cells.[8] This thesis offers a basic overview into the general principle in DSSC, in terms of the way it operates, assessment of performance with an emphasis on the most-latest developments, and production limitations are crucial factors that affect how effective DSSC is.

## **1.2. Solar cell types**

Based on their performance and requirements, solar cells are broadly categorized into three groups. Fig 1.4 shows how their categorization is represented in a tree graph.

### **1.2.1. First-Generation Solar Cell**

First-generation solar cells are made on silicon wafers, as was already explained. It is the most established and well-liked technology because of its excellent power efficiency. The following two subcategories are used to categorise silicon wafer-based technology: [9].

- Mono/ Single-crystalline silicon solar cell.
- Multi/Poly-crystalline silicon solar cell.

The Czochralski technique is used to produce silicon single crystals into monocrystalline solar cells, as the name implies. The large-sized ingots are cut into

Si crystals during the manufacturing process. As "recrystallizing" the cell involves more steps and is more expensive, these big single crystal manufacturing require careful processing. Mono-crystalline solar cells, which are fabricated from single-crystalline silicon, have an efficiency between 17% and 18% [10].

In a single cell, polycrystalline PV modules often consist of several distinct crystals that are connected to one another. Polycrystalline silicon solar cells are fabricated in a graphite mold by solidifying molten silicon, and perhaps produced at a lesser cost in comparison to mono-crystalline cells. The most popular solar cell type right now is polycrystalline Si. According to estimates, they constituted up to 48 percent of the solar cells produced globally in 2008. Different crystal structures are formed during the solidification of the molten silicon. They are less efficient than monocrystalline silicon solar panels by about 12% to 14%, although being slightly less expensive to manufacture.[11]

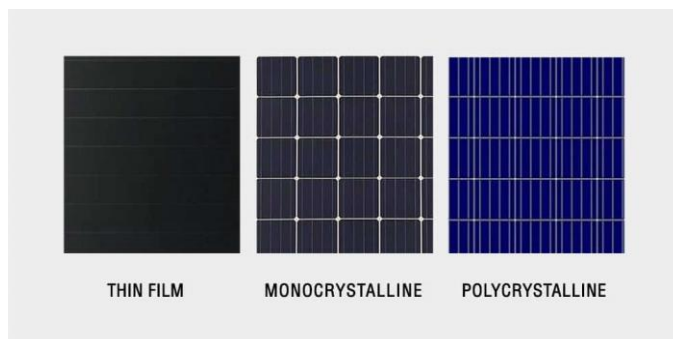


Figure 1.5 Monocrystalline and Polycrystalline solar cell [11].

### 1.2.2. Second Generation Solar Cell.

Most second-generation solar cells, including a-Si and thin-film solar cells, are typically more economical in comparison to first-generation silicon wafer solar cells. When compared to silicon-wafer solar cells, which are having light-absorbing layers up to 350  $\mu\text{m}$  thick, thin-film solar cells usually possess light-absorbing layers as thin as 1  $\mu\text{m}$  [12]. Three types of thin-film solar cells are identified, namely:

- a-Si

- CdTe
- CIGS (copper indium gallium di-selenide).

Low processing temperatures make it possible to create amorphous (a-Si) solar cells, which allows for the utilization of a distinct inexpensive, flexible substrates made of polymers. When referring to solar cells, the term "amorphous" denotes silicon material that is not highly structured, does not have a crystalline structure, and lacks a clear atomic arrangement in the lattice. They are manufactured by coating the substrate or back of a glass plate with doped silicon material. Presently, commercial PV modules' efficiency range from 4% to 8% [13].

Thin-film solar cells include cadmium telluride (CdTe), that is regarded as a major competitor for the evolution of cost-effective, commercially feasible photovoltaic (PV) devices. The first PV technology that could be produced more affordably was this particular one. Cadmium sulphide is sandwiched between layers to create a p-n junction diode. CdTe has a high absorption coefficient of more than  $5 \cdot 10^{15}/\text{cm}$  and a direct optimum band gap of about 1.45 eV [14]. Therefore, it normally has an efficiency of between 9% and 11% [15].

The four elements Copper, Indium, Gallium, and Selenium combine to form the quaternary compound semiconductor known as Copper Indium Gallium Di-Selenide (CIGS). The direct band gap semiconductors include CIGS as well. The efficiency of CIGS, which is higher compared to that of the CdTe thin film solar cell, is 10%–12%. CIGS is manufactured via a variety of methods, including sputtering, evaporation, electrochemical coating, printing, and electron beam deposition. [16].

### **1.2.3. Third generation solar Cell**

Third-generation cells are a unique novel technology, however they haven't been well studied on the commercial front. The majority of the established varieties of third generation solar cells are

1. Nanocrystal based solar cells (7% -8%)
2. Polymer based solar cells (3% - 10%)

3. Dye-sensitized solar cell (organic solar cell) (14%)
4. Concentrated solar cells
5. Perovskite based solar cells (organic-inorganic solar cells) (23.3%)

This generation uses a number of novel materials other than silicon, such as nanotubes, organic dyes, conductive polymers, quantum dots, and perovskites. Most of this generation's technology is still under development in laboratories, making the majority of it commercially unavailable. They are referred to as "emerging technology" because of its low market captivity. Polymer solar cells have the benefit of flexibility because of the polymer substrate, easy and large-scale production. The perovskite-based solar cell is the most recently developed among these third generation solar cells because it set a record efficiency beyond 23% [17] on a very tiny area in a short span of research time but was unable to be commercialized due to stability and toxicity concerns.

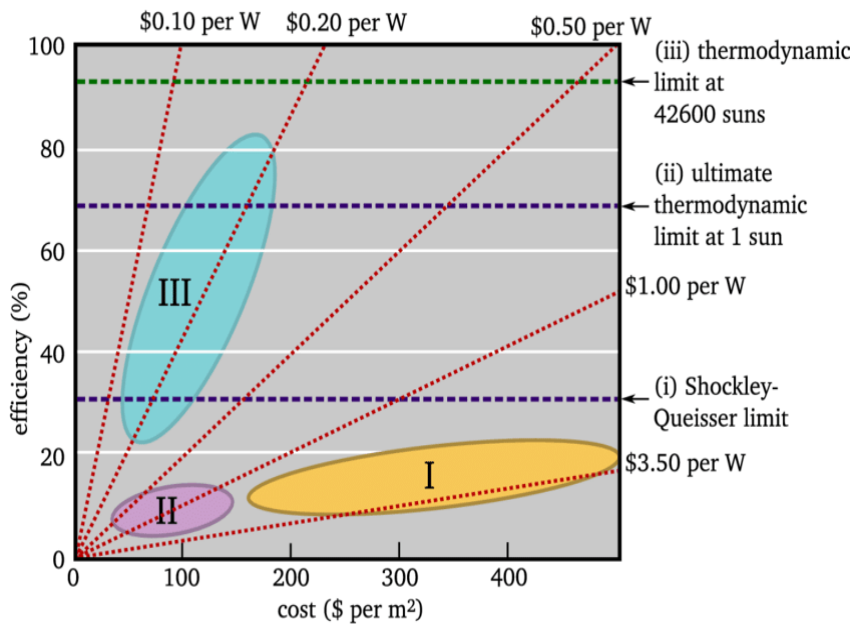


Figure 1.6 Efficiency versus price per watt for 3 different generations [17].

### 1.3. Dye sensitized solar cell

In 1988, Brian O'Regan along with Michael Gratzel at UC Berkeley co-invented Gratzel cells, also known as Modern Dye-Sensitised Solar Cells (DSSCs).

The prototype DSSC had been reported by Michael Gratzel in 1991. These cells which replicate the photosynthesis in plants by sensitizing nano-particulate titanium dioxide ( $\text{TiO}_2$ ) films with a new ruthenium (Ru) bipyridyl complex. This absorbed energy is enough to knock an electron from the excited chlorophyll. DSSCs use a sensitizer and nanoparticles of the semiconductor like Titanium dioxide ( $\text{TiO}_2$ ) to transform luminous energy into electrical energy. Between the two electrodes within a solution of electrolyte that consist of iodine ions,  $\text{TiO}_2$  nanoparticles sensitized with a dye absorb a broad range of wavelengths

Dye Sensitized solar cells (Third generation Solar Cells) are known for their clean, sustainable and renewable sources of energy. They can convert sunlight into electrical energy by means of photovoltaic effect. They attracted researchers attention because they are easy to manufacture, transparency and colour. In the initial days, when ruthenium dyes were used along with iodide electrolyte, the power conversion efficiency of DSSCs observed was 11.9% [18]. Due to the third-generation cells' (DSSC) low manufacturing costs and minimal environmental impact, extensive research has been conducted on them.

Solar energy is transformed into electrical energy by employing dye-sensitized solar cells. They mimic how solar energy is captured by plants. In a DSSC, a dye produces electrons when it absorbs light. To absorb visible light, the dye has a conjugated system, which has alternate single and double bonds. The perfect sensitizer in case of dye-sensitized solar cells must be strongly attached to the surface of semiconductor oxide, absorbing all light below a threshold wavelength of 920 nm, as well as inject electrons into the conduction band having a yield quantum of unity. [19].

#### **1.4. DSSC Structure and Working concept;**

The fabrication of third-generation solar cells, namely DSSCs, is done to reduce costs and is based on a straightforward, inexpensive, as well as simple

manufacturing technique. These DSSCs could probably be an alternative to Silicon Solar cells in the due to its effectiveness as well as their efficiency.

A mesoporous oxide layer-based photoanode based on nanomaterials, a monolayer of dye molecules acting as an absorber, an electrolyte of redox couple, as well as a catalytic counter electrode composed of conductive glass comprise the configuration of DSSCs. Titanium dioxide (anatase, rutile, or a combination of both) is the most researched photoanode material for DSSC application due to their greater activity for catalysis, simplicity of synthesis, low cost, non-toxicity, and chemical stability while exposed to radiation [20].

In the DSSC, there is an excitation of dye molecules by light as it travels through the transparent anode. Electrons are injected into the semiconductor-like  $\text{TiO}_2$ ,  $\text{ZnO}$ , or  $\text{SnO}$  layers by excited molecules of dye. Before coming back to the redox (Iodide) electrolyte, the electrons move from the counter electrode to the external circuit. The electrolyte then transports the electrons back to the dye molecules. A photosensitizer needs to possess these features in order to be effective:

- 1) It should absorb visible wavelengths between 400 and 700 nm.
- 2) High extinction coefficient
- 3) Adsorb to a greater extent on the surface of the  $\text{TiO}_2$  semiconductor
- 4) stability in an oxidised state, enabling reduction by an electrolyte;
- 5) stable enough to last for almost 10<sup>8</sup> revolutions, or 20 years of cell operation [21];

A DSSC designed like a sandwich consists of 5 components as shown in fig1 :1) A conductive transparent thin film (ITO or FTO) deposited on a glass substrate which serves as photoanode. Most of the ITO films applied are annealed not only to lower the number of defects but also to enhance the electrical conductivity.2) A semiconductor thin film which is nano crystalline in nature. A dye which is used as a light harnessing element. 3)A redox Electrolyte 4) As a counter electrode, conductive glass which has either a carbon or platinum coating is used. This process

of DSSC begins when the dye sensitizer absorbs the photons. When electrons undergo excitation from its highest occupied molecular orbital (HOMO) to their lowest unoccupied molecular orbital (LUMO), which separates the charge between the dye and the  $\text{TiO}_2$ , the molecules of dye get injected into the semiconductor's conduction band. The dye is oxidised by the redox electrolyte when electrons are regenerated from the HOMO state, and the process repeats in which the regenerated electrons produced at the starting travel through the external circuit from the photoanode to counter electrode. When the energy level of the dye's highest occupied molecular orbital (HOMO) is lesser than the electrolyte's redox potential and that of its lowest unoccupied molecular orbital (LUMO) is greater in comparison to conduction band of  $\text{TiO}_2$ , the dye can regenerate more effectively. [22].

The minute energy packets of Electromagnetic radiation are called as photons (light quantum). When the sensitized dye is absorbed by the photon, there is an excitation of HOMO electron and it reaches LOMO. From the LUMO, an excited electron is injected into the semiconductor's conduction band [23].

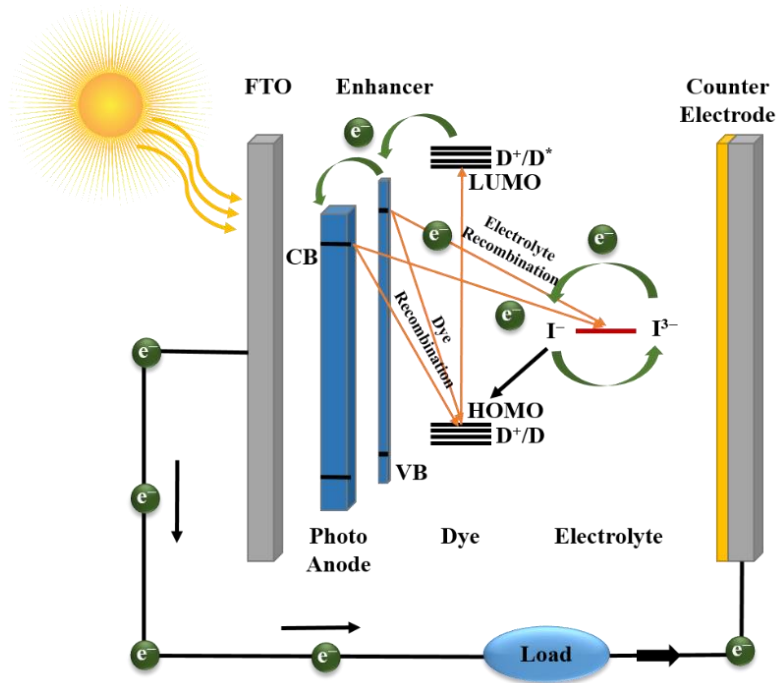


Figure 1.6 Schematic working mechanism illustration of the dssc [50]

## **1.5. Photovoltaic parameters of DSSC**

The main photovoltaic characteristics employed to describe how solar cells work under irradiation are open circuit voltage ( $V_{oc}$ ), short circuit current ( $J_{sc}$ ), power conversion efficiency ( $\eta$ ), as well as fill factor (FF).

### **1.5.1. Short circuit current**

The  $J_{sc}$  of the solar cell is determined by the charge carrier mobility of the layer that is active. When zero bias is applied, the photogenerated current density of the cell is referred to as its short circuit current density ( $J_{sc}$ ). Charge transport and exciton dissociation take place because of the development of built-in potential. A DSSC's  $J_{sc}$  is influenced by both excitons generated and incident light. When a photoactive layer with a wide absorption spectrum gathers more excitons from the terrestrial solar spectrum, the DSSC's  $J_{sc}$  is at its highest. [24].

### **1.5.2. Open circuit voltage**

In order to remove the current produced during radiance, solar cells are exposed to an open-circuit voltage ( $V_{oc}$ ). Solar cells receive a bias voltage, often known as an open-circuit voltage ( $V_{oc}$ ). When it is dark, the external current ( $J = 0$ ) stops flowing at the  $V_{oc}$ . The  $V_{oc}$  is dependent on the Fermi energy's work function (Fermi energy refers to the highest energy level that a material experiences at absolute zero kelvin) of the working electrode and electrolyte. The  $V_{oc}$ , experimentally determined is a bit low due to the charge carriers recombination whereas when all recombination processes are minimized, only then is the theoretical limit reached. [25].

### **1.5.3. Fill factor**

The primary function of a solar cell, often referred as a photovoltaic cell, is to transform the energy of light into electric power. The greatest power conversion efficiency (PCE) of a solar cell is determined from its J-V curve (Fig. 7). The

product of open circuit voltage as well as short circuit current yields FF, which has the maximum power possible.

With the help of FF, the evaluation of diode characteristics can be made. The FF needs to be unity for a diode to be ideal. More perfect the diode is, the higher the FF. The FF was determined to be between 0.6 to 0.85 because of transport losses and recombination. [26]

$$FF = \frac{V_m I_m}{V_{oc} I_{sc}} \dots \dots \dots \text{Eq. (3)}$$

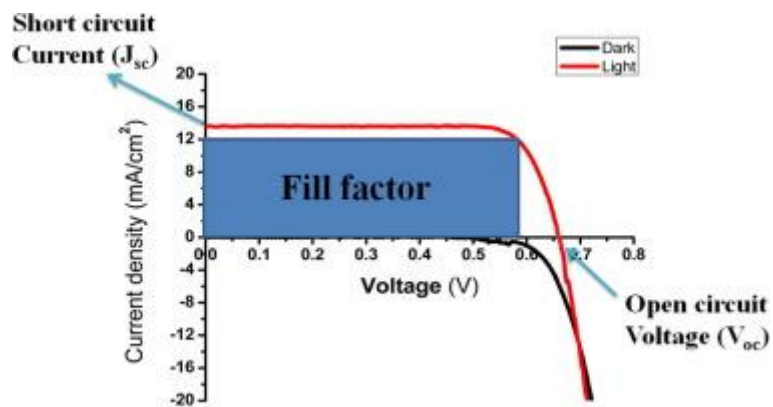


**Fig.1.7: J-V Characteristic curve of DSSC[26]**

#### 1.5.4. Efficiency

A DSSC's efficiency is calculated by dividing the power generated that is maximum ( $P_{max}$ ) by the power of incident light ( $P_{in}$ ). The PCE ( $\eta$ ) is the maximum efficiency of the DSSC that converts light energy into electrical energy [27].

$$\eta = \frac{P_{max}}{P_{in}} = \frac{FF \times Voc \times Jsc}{Pin}$$

Eq. (4)

Where,

$V_m$  – Maximum value of voltage,

$I_{sc}$  – Short-circuit current,

$I_m$  – Maximum current value,

$\eta$  – Efficiency of the cell,

$V_t$  – Terminal voltage of the cell

$V_{oc}$  – Open-circuit voltage.

## **1.6 Thesis structure**

The structure of this thesis is as outlined below:

1. Chapter 1 explains what a solar cell is, the different solar cells types, dye-sensitized solar cells (DSSCs), their components, and their operating principles.
2. Chapter 2 provides a summary of prior work, obstacles encountered in the field of dye-sensitized solar cells, motivation, along with work objectives.
3. In Chapter 3, experimental methods were explored, including the manufacture of  $\text{TiO}_2$  nanorods and the preparation of an electrolyte and cocktail of natural dyes.
4. Chapter 4 reviewed the outcomes of several methods for characterising the numerous layers that had been deposited on substrates.
5. Chapter 5 summarises the study's results, plus future prospects are discussed.

## Chapter 2

### 2. Analysis of Previous Research Work and approach to Problem

Researchers have focused a greater emphasis on DSSCs among third-generation solar cells because of their ability to provide economical, adaptive, and extremely effective conversion of solar energy. The development of DSSCs commenced in the beginning of 1990s, from that time there were many substantial achievements in terms of performance. In the first ten years of research, the DSSCs power conversion efficiency (PCE) rose from a mere 1% to over 10%. In this chapter, we shall go through the the prior research on dye-sensitized solar cells along with their advancements.

#### 2.1.1. Past research activity on dye-sensitized solar cells:

This research discusses the evolution of novel materials for effective, excellent performing dye-sensitized solar cells (DSSCs) providing a replacement to solar cells made of silicon. A power conversion efficiency of 6.92% had been achieved in the outstanding research carried by O'Regan and Gratzel using dye-sensitized nano-rods of titanium dioxide (TiO<sub>2</sub>) film as the electron transport layer. This sparked significant interest in DSSCs. Despite testing a variety of semiconducting oxides in DSSCs, the most efficient photoelectrode was found to be the TiO<sub>2</sub> nanoparticle-based electron transport layer.[28] The DSSC system consists of five components, which are described below.

- ❖ Glass substrate
- ❖ Photo anode
- ❖ Natural dye
- ❖ Electrolyte
- ❖ Counter electrode.

#### 2.1.2. Glass substrate:

Due to its greater efficiency as well as transparency, fluorine-doped titanium oxide (FTO) is primarily used substrate that is employed in dye-sensitized solar

cells (DSSCs). This characteristic renders it an essential choice for researchers investigating DSSCs.

### **2.1.3. Photo anode made by semiconductor:**

Semiconductor materials like chalcogenides,  $\text{TiO}_2$ ,  $\text{ZnO}$ , and  $\text{SnO}_2$  have been extensively investigated for their wide utility in energy storage applications. Dye-sensitized solar cells (DSSCs) had been evaluated utilizing various semiconducting oxides as photoelectrodes. However, the most efficient electron transport layer utilized in DSSCs is based on titanium dioxide ( $\text{TiO}_2$ ) nanoparticles, which function as sensitizers to simplify light-induced redox processes because of the electronic structure that is conductive, comprising of conduction band (CB) as well as valence band (VB) [29].  $\text{TiO}_2$  exists in three distinct natural forms, as listed below. The following table displays some of the potential combinations.

1. Rutile.
2. Anatase.
3. Brookite.

Titanium dioxide ( $\text{TiO}_2$ ) is present in 3 major phases: anatase, rutile, along with brookite. The most stable phase of titanium dioxide, rutile, has been expected to remain stable at all temperatures. However, Anatase is known to be more active in terms of physical and chemical activity, making it the preferred choice in case of dye-sensitized solar cells.  $\text{TiO}_2$  acts as a sensitizer for light-induced redox reactions due to its electronic structure that is conductive, comprising of conduction band (CB) along with valence band (VB). An electron gets excited into the conduction band and leaves a hole with a positive charge in the valence band when light with energy exceeding or corresponding to the bandgap ( $E_g$ ) strikes the surface of a semiconductor. These charges can be utilized to generate an electric current for an external load.



Figure 2.1. Schematic representation for fabrication of DSSC[50]

It has been proposed that a semiconductor with a larger surface area, which is porous, and has features that align with the sensitizer can increase the dye-sensitized solar cells (DSSCs) efficiency. The best suitable semiconductor for this purpose has been identified to be titanium dioxide ( $\text{TiO}_2$ ). According to literature, the highest efficiency achieved by DSSCs to date is approximately 7%, which was obtained using Z907 dye in conjunction with a platinum counter electrode. Figure 2.1 illustrates the schematic representation for fabrication of DSSC.

Table1: Comparison of TiO<sub>2</sub> for DSSC and Characteristics

Photo anode	Counter Electrode	Technique	Dye	V <sub>oc</sub> (mV)	J <sub>sc</sub> (mA cm <sup>-2</sup> )	FF	η (%)	Ref.
TiO <sub>2</sub>	pt	Sol-gel dip coating	Red cabbage	470	4.38	0.36	0.73	[17]
TiO <sub>2</sub>	pt	Sol-gel dip coating	Blue pea	450	4.16	0.35	0.67	[17]
TiO <sub>2</sub>	Graphite	-	Lawsone	330	0.38	0.57	0.7	[18]
TiO <sub>2</sub>	Graphite	-	Sumac	390	0.93	0.41	1.5	[18]
TiO <sub>2</sub>	Graphite	-	Curcumin	280	0.20	0.65	0.36	[18]
TiO <sub>2</sub>	pt	Screen printing	Mangosteen peel	570	4.72	0.54	1.47	[19]
TiO <sub>2</sub>	PEDOT-PSS	“	“	580	3.88	0.27	0.60	[19]
TiO <sub>2</sub>	Pt	“	“	620	5.40	0.52	1.75	[19]
TiO <sub>2</sub>	PEDOT-PSS	“	“	580	4.33	0.35	0.88	[19]
TiO <sub>2</sub>	Carbon black	Doctor blade	G.atroviridis	320	2.55	0.63	0.51	[24]
TiO <sub>2</sub>	“	“	E.Conferta	370	6.56	0.49	1.18	[24]
TiO <sub>2</sub>	Pt	“	pomegranate	460	0.62	0.55	1.57	[26]
TiO <sub>2</sub>	Pt	Constant current(EP P)	Cosmos	447	1.041	0.61	0.54	[25]
TiO <sub>2</sub>	“	“	Golden Trumpet	405	0.878	0.54	0.40	[25]
TiO <sub>2</sub>	Pt	“	Bouginevill	859	0.898	0.52	0.38	[25]
ZnO	C	Sol-gel spin coating	Jamun	580	1.56	0.58	1.23	[29]
ZnO	Graphite	Spin coating	Beetroot	380	5.45	0.36	0.75	[30]

TiO <sub>2</sub>	Pt	Spin coating	Z907	691	14.1	0.71	6.92	[34]
------------------	----	--------------	------	-----	------	------	------	------

#### 2.1.4. Dye

##### **material**

A variety of naturally occurring materials, including fruits, flowers, leaves, and microbes, contain pigments that exhibit a diverse range of colors. These pigments can be extracted from these sources with ease and have potential for utilization in Dye-Sensitized Solar Cells (DSSCs).

Due to the high visible absorption coefficients, availability, easy manufacturing, plus environmental friendliness in natural dyes, they are attractive for use as photosensitizers in dye-sensitive solar cells (DSSCs). The fact that noble metals like Ru are not required, making the process more cost-effective, is a significant benefit of natural dye-based DSSC synthesis.

In a comparative analysis of synthetic and natural sensitizers, various factors like cost, environmental challenges, maximum absorbance, stability issues, DSSC efficiency, resource availability, and cell manufacturing processes were considered. Metal complex sensitizers require a complex fabrication process, while natural sensitizers can be obtained from sources like leaves, flowers, and roots using a simple extraction process involving ethyl alcohol, methyl alcohol, or water. As a result, natural dyes are less expensive than synthetic ones [35]. Research has shown that throughout the year, adequate quantities of wildflowers, particularly *Ixora Coccinea*, leaves of Spinach are available, which could potentially reduce the overall cost of DSSCs.

##### **2.1.5. Electrolyte**

An electrolyte is a crucial component of a DSSC that significantly affects the cell's overall efficiency and long-term stability. Typically, electrolytes consist of three components: a redox pair, an organic solvent, and additives. The three different electrolytes are as follows: (i). liquid electrolyte, (ii) solid electrolyte as well as (iii) quasi-solid electrolyte. Butyrolactone, propylene carbonate, ethylene carbonate, and 3-methoxy propionitrile are the most often utilised solvents in the liquid

electrolyte. A DSSC's photoelectric performance is determined by the solvents' dielectric constant, viscosity, and donor number. The electrolyte's redox pair functions as both an oxidising and a reducing agent. Due to their improved cell performance,  $I^-/I^3^-$  and  $Co(II)/Co(III)$  are the two redox couples that are most frequently utilised in DSSC. The recombination reactions at the interface of the semiconductor-electrolyte are prevented by additives, and thus it improves the cell performance.[36]

## **2.2. Work motive:**

This study is motivated by the significant achievements of dye-sensitized solar cells within a decade of experimental research, as well as the current challenges and limitations associated with these cells. However, commercialization of these cells is hindered by stability issues and limited lifetime, particularly with respect to the use of liquid electrolyte materials. Despite attempts by some researchers to develop solid electrolyte-based dye-sensitized solar cells, they still had trouble maintaining their efficiency. To better the effectiveness, stability, along with economic viability of dye-sensitized solar cells, this work will investigate and address these challenges.

Through analysis of various literature, it has been observed that the impressive efficiency of dye-sensitized solar cells (DSSCs) is associated with the use of mesoporous  $TiO_2$  as a photoanode material in conjunction with dye, as well as the incorporation of either nickel or carbon as counter electrode during fabrication. In light of this, the current research is aiming for increasing the functionality of DSSCs by optimising the diameter as well as length of  $TiO_2$  nanorods.

- Dye-sensitized solar cells (DSSCs) are not only biodegradable but also benign to this environment. Furthermore, the synthesis process involved in fabricating DSSCs is relatively simple and involves less cost.
- Reduced production and material costs, along with enhanced device functionality, are essential for increasing the commercial viability of dye-sensitized solar cells (DSSCs).
- The synthetic dye used in dye-sensitized solar cells (DSSCs), that was made using toxic materials, constitutes one of the majority of costly components since it requires complex processing.
- Natural sensitizers for dye-sensitized solar cells (DSSCs) are not only readily available but also are easily derived from an array of plant sources, including leaves, fruits, and flowers.
- Dye-sensitized solar cells (DSSCs) exhibit a higher energy conversion efficiency than other solar cell technologies at higher temperatures, in diffuse light, and when it is cloudy or overcast.

### **2.3. Objectives:**

Considering the facts mentioned above, the following objectives are being pursued:

- The objective is to synthesise  $\text{TiO}_2$  nanorods using a hydrothermal method that is economical.
- The aim is to extract a natural dye through the employment of a cocktail of *Ixora Coccinea* flowers and *Spinacia oleracea* leaves.
- The objective is fabricating an efficient dye-sensitive solar cell (DSSC) using a blend of environmentally friendly dyes, as well as to optimize and evaluate the relevant parameters.

In this chapter, a literature survey was conducted to identify suitable materials that would work well for making dye-sensitized solar cells.  $\text{TiO}_2$  is selected as a photoanode material, while nickel and carbon were chosen as the counter electrodes. Additionally, a promising natural dye for the dye-sensitized solar cell was identified in a mixture of *Ixora coccinea* along with *Spinacia oleracea*.

## Chapter 3

### Experimenting Techniques

This chapter pertains to the methodologies employed in the fabrication and analysis of materials.

#### 3.1 Experimenting Techniques:

##### 3.1.1. Process of Spin coating

Spin coating is a commonly employed solution-based technique for depositing uniform thin films onto substrates using centrifugal force. This process involves spinning a solution of the material and solvent at high speeds, during which the surface tension and centripetal force of the liquid work together to produce a uniform layer ranging in thickness from a few nanometers to a few microns. This technique comprises of four steps: spin up, deposition, spin off, as well as evaporation, as illustrated in Figure 3.1. To begin, the FTO substrate is placed onto the vacuum turntable of the spin coater and a little amount of the solution material is coated onto the substrate. The solution is then distributed on the substrate by centrifugal force, and high spinning speeds cause the layer to thin. Following this, the layer is dried to remove volatile components and achieve uniform evaporation. In this research, a rotation speed of 3000 rpm for 30 seconds was utilized to obtain a uniform  $\text{TiO}_2$  compact layer film having thickness of approximately 80 nm.[37] The absorber layer along with hole transport layer had been also coated using this spin coating technique with an appropriate rotation speed.

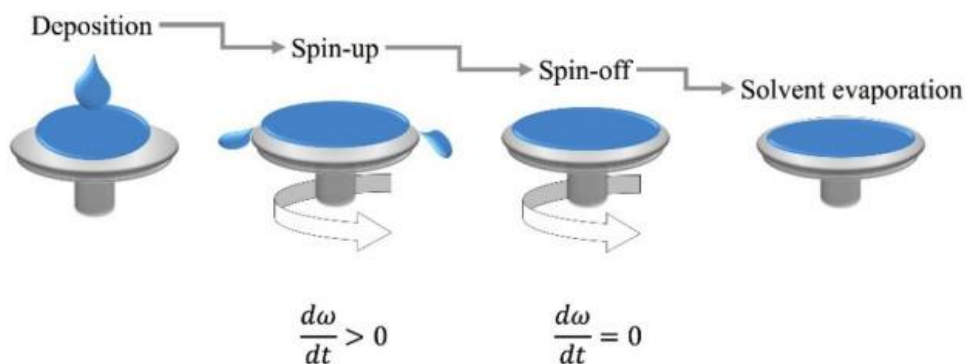


Figure 3.1 Stages of spin coating technique on substrate [38]

### 3.1.2. Hydrothermal Synthesis method

Hydrothermal synthesis is a significant method for producing nanostructured materials that find their uses in various fields like electronics, optoelectronics, as well as energy storage devices. The term "hydrothermal" has a Greek origin, where "hydro" means water, and "thermos" refers to heat. The term "hydrothermal reaction process" refers to any chemical reaction that takes place at high pressures and temperatures comprising water (deionized water). The reaction is carried out in a sealed vessel, called an "autoclave," which can withstand highly corrosive solvents at high temperatures and pressures. Typically, stainless steel is used to make the autoclave. A Teflon-lined beaker is used to protect the main part of the autoclave from highly corrosive substances and extreme pH conditions.[38] The Teflon beaker is filled with the precursor solution, consisting of deionized water, which is then put into the stainless steel autoclave. The autoclave that is well sealed is put inside an oven at the desired temperature. One of the key advantages of this method compared to others is its capability to produce crystalline phases that are unstable at the melting point. This method enables the growth of large, high-quality crystals through precise control of crucial parameters like reaction duration, temperature, as well as the concentration of precursors and solvents. In this research work, the hydrothermal technique was used to synthesize well-oriented, one-dimensional TiO<sub>2</sub> nanorods whose length and diameter were controlled by varying the reaction time.

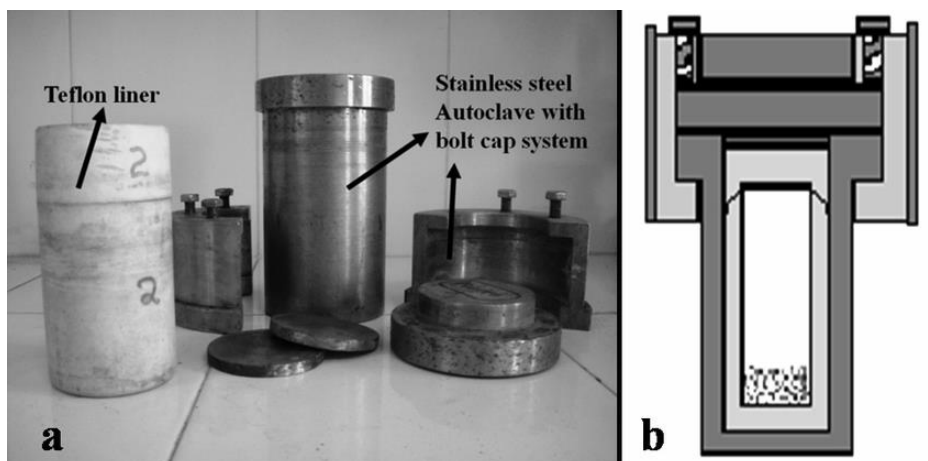


Figure 3.2 a) Teflon liner and b) Stainless steel Autoclave[38]

### 3.2. Synthesis and design of dye-sensitized solar cell

The production of dye-sensitized solar cells involves several steps. First, the FTO glass substrate is cleaned using ethanol, DI water, and acetone to remove any contaminants. Then, a  $\text{TiO}_2$  compact layer is synthesized and deposited onto the substrate. Next,  $\text{TiO}_2$  nanorods are synthesized and deposited onto the compact layer.

After that, a cocktail of natural dye is derived from flowers of *Ixora Coccinea* and leaves of *Spinacia oleracea*, as well as the dye is deposited onto the  $\text{TiO}_2$  nanorods. The synthesized electrolyte is then prepared and applied to the dye-sensitized  $\text{TiO}_2$  nanorods.[3]

Finally, the nickel and carbon are cleaned and used as the counter electrode. These steps are necessary for producing a dye-sensitized solar cell that are not only functional but also effective at converting light from the sun into electric power.

**Materials:** In the manufacturing process of dye-sensitized solar cells, fluorine-doped tin oxide (FTO) has been employed as the substrate, while titanium diisopropoxide bis(acetylacetonate) and titanium butoxide serve as the precursors for the compact layer and TiO<sub>2</sub> nanorods (TNRs) coating, respectively. Solvents such as 1-butanol, hydrochloric acid, DI water, and ethylene glycol are utilized, while the extraction of natural dyes from spinach and ixora coccinea, potassium iodide, iodine crystals, carbon, and Ni-based counter electrodes are used as additional components. All the materials employed in the process had been obtained from Sigma-Aldrich, as well as were of analytical grade, meaning they met the highest purity standards available in the market, and were used without any further refinement. These materials were essential to the manufacturing technique's success since they ensured the finished dye-sensitized solar cell's quality and reproducibility

### **3.2.2. FTO glass substrate cleansing**

The FTO-coated glass substrate was initially provided as a 100 mm x 100 mm sheet, then subsequently sectioned into smaller pieces measuring 15 mm x 15 mm. The cleaning process involved the following sequential steps:

1. FTO glass substrates were treated with ultrasonic waves in a bath of deionized (DI) water for 15 minutes after being first cleaned with soap.
2. In the subsequent step, the substrates were subjected to ultrasonic treatment in acetone for a duration of 15 minutes to eliminate any residual grease, dust, and chemicals from the previous step.

3. Following that, the substrates underwent another ultrasonic treatment, this time in ethanol for a duration of 15 minutes. This step was aimed at removing carbon-related impurities that may have accumulated on the surface during the acetone cleaning process.

4. Finally, the substrates were dried using a hot air blower and then put down onto a hot plate and heated to 120 °C for a duration of 30 minutes. This step was intended to remove any residual organic solvents present on the substrates. [39].

### **3.2.3. Fabrication of compact (c) TiO<sub>2</sub> layer and TiO<sub>2</sub> Nanorods**

The synthesis of TiO<sub>2</sub> nanorods (TNRs) as a photoanode involved the preparation of clean FTO substrates in an ultrasonic bath with soap, DI-water, acetone, as well as ethanol to eliminate surface contaminants. The compact layer of TiO<sub>2</sub> (c-TiO<sub>2</sub>) has been synthesized by spin-coating 0.15M and 0.30M of Titanium diisopropoxide bis(acetylacetonate) solution in 1-butanol solvent once and twice, respectively [40]. The substrates were then heat-treated at 120 °C for 30 mins, then annealed at 450 °C for 30 mins to attain a uniform, dense layer of c-TiO<sub>2</sub>, which served as a seed layer for TNR growth. The TNRs were prepared using a one-step hydrothermal technique by dissolving 0.75 ml Ti(OBu)<sub>4</sub> in a solution of DI-water and HCl (1:1 v:v), stirring the solution at room temperature for 30 mins, subsequently pouring it into a Teflon liner with the FTO substrate which faces downwards. The liner was sealed in an autoclave as well as heat-treated at 150 °C for 8h. The samples had been cleansed using DI water and air-dried before being annealed for 30 mins in a muffle furnace at 450 °C. The synthesis process was simply depicted in Figure 3.3

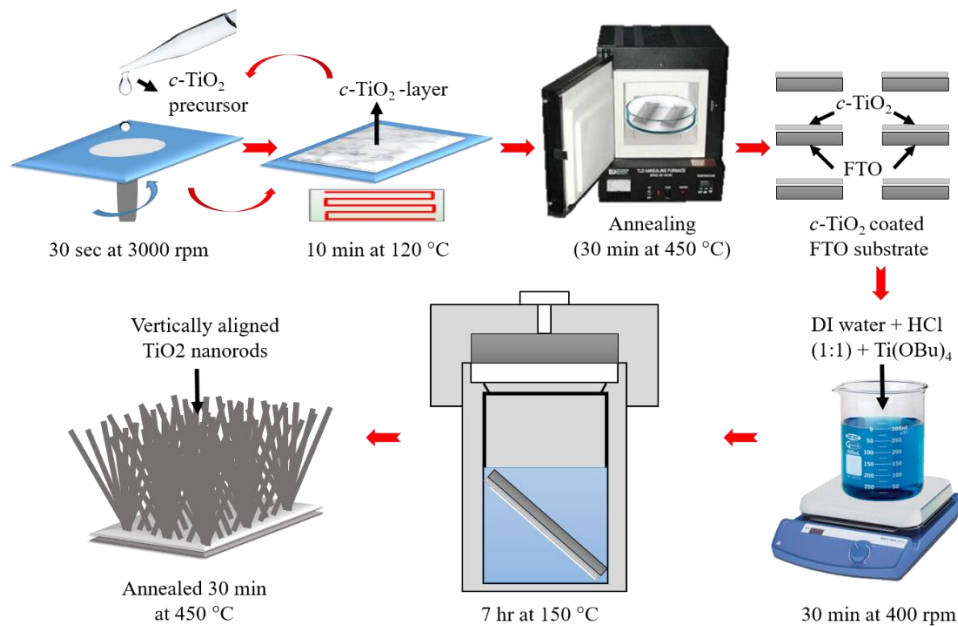


**Figure 3.3.** TiO<sub>2</sub> coated FTO glass substrate after hydrothermal synthesis

### 3.2.4. Preparation of Cocktail of Natural dyes

In order to create dye-sensitized solar cells (DSSCs), care must be taken that we select the right dye because it greatly affects the device's performance, ease of synthesis, stability, adjustability, cost-effectiveness, and compatibility with the environment. [5]. In this study, two different natural dyes and cocktail of natural dyes was chosen for device fabrication, and the dyes were extracted using *Ixora Coccinea* flowers and Spinach leaves using the following process:

1. The initial step in the extraction of natural dye from flowers involved washing the flowers with normal water to eliminate any visible dust and removable impurities adhering to the surface of the flowers.
2. To further remove impurities from the flowers, they were sonicated in deionized (DI) water for a period of 7 minutes. This process involved subjecting the flowers to high-frequency sound waves in the presence of DI water, which facilitated the removal of impurities through mechanical disruption.

3. Following the washing and sonication steps, the *Ixora coccinea* flowers were ground to extract the dye. The extraction process involved using an appropriate amount of deionized (DI) water as a solvent to facilitate the dissolution of the dye molecules from the flower. The grinding process was carried out to increase the surface area of the flowers and ensure efficient extraction of the dye, allowing for greater contact between the solvent and the dye molecules.
4. The aforementioned extraction process was also repeated for the leaves of spinach. The spinach leaves were subjected to washing, sonication, and grinding steps similar to those described above for the *Ixora coccinea* flowers. An appropriate amount of DI water was used as a solvent during the grinding step to ensure efficient extraction of the dye from the spinach leaves.
5. After the extraction process, the dye solution obtained from both the *Ixora coccinea* flowers and spinach leaves was subjected to centrifugation to remove any solid sediments. This involved subjecting the solution to a high-speed rotational force that caused the solid particles to separate and settle at the bottom of the container. Following centrifugation, the dye solution was filtered utilizing a coffee filter paper to eliminate any remaining solid impurities and obtain a pure dye solution.
6. To obtain a concentrated form of the extracted dye, the dye solution was subjected to an evaporation process. This involved the use of an evaporator to remove the solvent from the dye solution, leaving behind a pure and concentrated dye extract.

### **3.2.5. Preparation of Electrolyte**

A previously described technique was used to create an electrolyte solution that contains iodine. 0.83 gms of potassium iodide along with 0.127 gms of iodine crystals were combined with 10 mL of ethylene glycol to create a homogenous mixture. To ensure uniformity, the mixture was spun

for 30 minutes. In order to prevent direct sunlight exposure, the resulting iodine electrolyte solution had been stored within an area of darkness with proper sealing [41].

### **3.2.6. Synthesis of Counter Electrode**

A nickel foam sheet of the same size as Fluorine-doped Tin Oxide (FTO) was compressed under pressure. The compressed nickel foam sheet was then washed with ethanol and sonicated for 5 minutes to eliminate any impurities present on the surface. This process was performed to ensure the cleanliness of the nickel foam sheet and prevent any contaminants from affecting subsequent processes. The carbon counter electrode is typically made from a conductive and porous material, such as graphite or carbon black.

## **3.3 Various analytical and Characterization Techniques**

### **3.3.1. Calculation of Fill Factor and Efficiency employing Current density – Voltage (J-V) curves**

A Solar simulator instrument was utilized to measure the J-V characteristics of a 1cm x 1cm sample under 1.5 G solar irradiation spectrum in both forward directions, using a 100 MW power. Dye-sensitized solar cells' stable power conversion efficiency (PCE) was determined by measuring the power output under a voltage that remained constant close to the maximum power point, while maintaining the device temperature at a constant value of 27°C. The primary aim of solar simulation technology is to create a laboratory-controlled indoor testing facility that closely resembles natural sunlight. A solar simulator is an apparatus that replicates sunlight in a laboratory setting, with a light source designed to have an

intensity and spectral composition similar to that of sunlight.

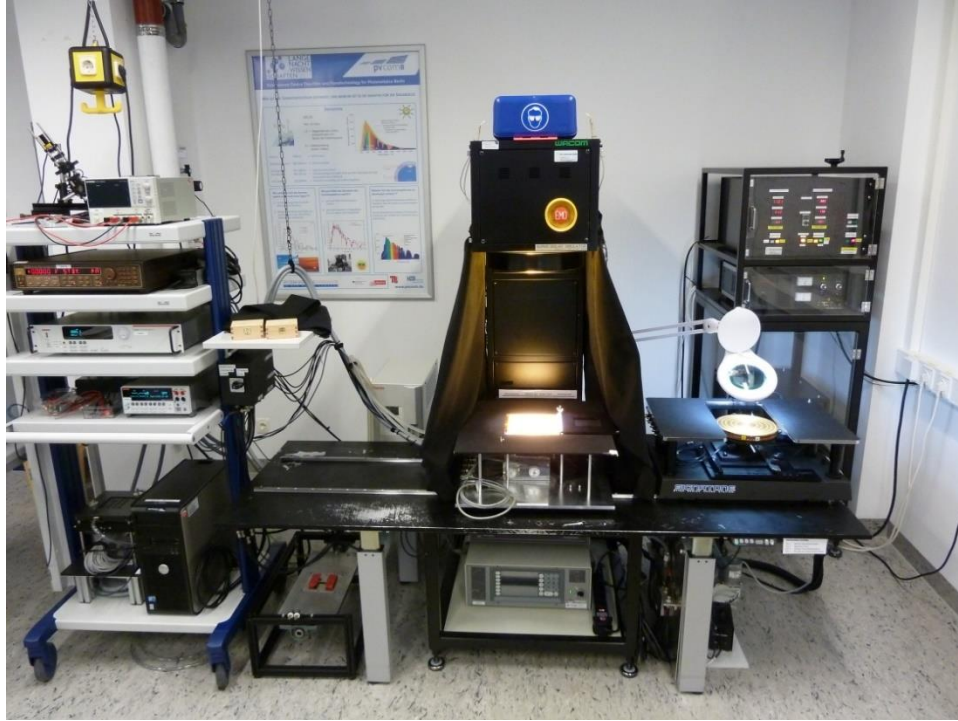


Figure 3.4. Schematics of solar simulator

### 3.3.2) X-ray diffraction (XRD)

X-ray diffraction (XRD) has become a popular and efficient non-destructive approach to identify crystalline materials. It gives detailed information on various structural parameters such as crystal structures, grain size, crystal defects, unit cell dimensions, and phases. X-rays are used in the XRD method to irradiate a sample, and the diffracted X-rays that interact with the crystalline structure of the sample are then measured. The atomic arrangement, crystal symmetry, and other structural details of the sample can be obtained by analyzing the diffracted X-ray pattern.

**Working Principle:** A material's crystal structure acts as a three-dimensional diffraction grating for X-ray wavelengths, as per the X-ray diffraction (XRD) theory. When X-rays are directed at a sample, they are scattered from an array of the lattice planes within the crystal structure at particular angles. If the

scattered beams interfere constructively, XRD peaks are formed. The distribution of atoms within the lattice determines the intensity of the peaks, which is unique to the crystal structure. Thus, XRD serves as a fingerprint of periodic atomic arrangements. Bragg's law, which relates the X-ray angle of incidence to the spacing between the lattice planes and the order of diffraction, describes the constructive interference condition. The Bragg's law equation can be employed to find the crystal structure of a material by analyzing the positions and intensities of the XRD peaks.

$$n\lambda = 2 d_{hkl}\sin\theta$$

where ' $n$ ' represents the order of diffraction (an integer greater than zero), ' $\lambda$ ' represents wavelength of incident X-ray, ' $d$ ' represents interplanar distances of lattice planes indexed by  $(h,k,l)$  & ' $\theta$ ' represents angle of incidence of X-ray beam with respect to lattice planes. Fig.3.5 depicts the X-ray diffraction obtained from the crystal lattice.

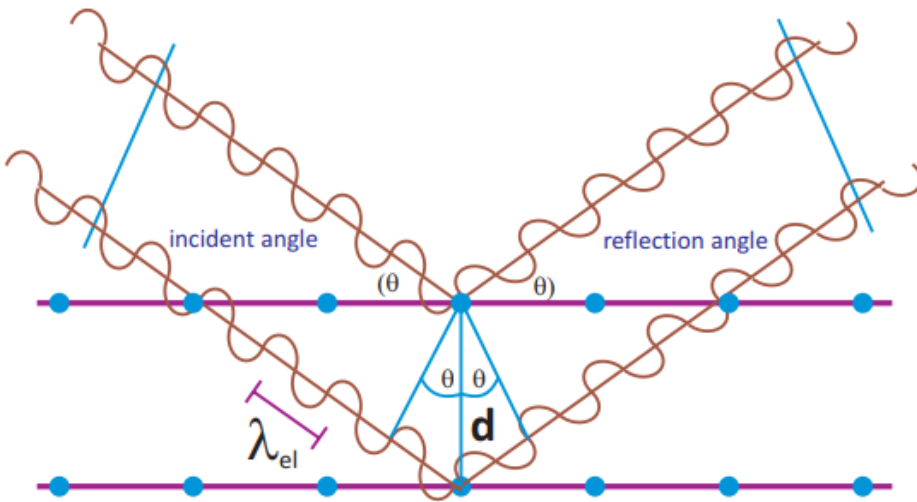


Figure 3.5 Schematic of X-ray diffraction [42]

### 3.3.2.1 Instrumental Arrangement:

The three essential components of an X-ray diffractometer are the X-ray tube, sample holder, as well as the detector. The cathode ray tube filament is heated to produce electrons that are accelerated in the direction of the target when a voltage is applying a voltage. When the electrons collide with the target material, they knock off inner shell electrons, producing characteristic X-ray spectra. Copper is the material that is primarily used for single-crystal diffraction due to its  $K\alpha$  radiation with a wavelength of  $\lambda = 1.5418 \text{ \AA}$ . The collimated X-ray beam is directed towards the sample, which is rotated along with the detector to record the intensities of reflected X-rays. When reflected rays interfere constructively, a peak in intensity appears. The detector then processes the X-ray signal, which is converted to a count rate and output provided to the user. The collimated X-ray beam hits the rotating sample at an angle  $\theta$ , and the detector collects the diffracted beams while rotating at an angle of  $2\theta$ , as illustrated in figure 3.6.

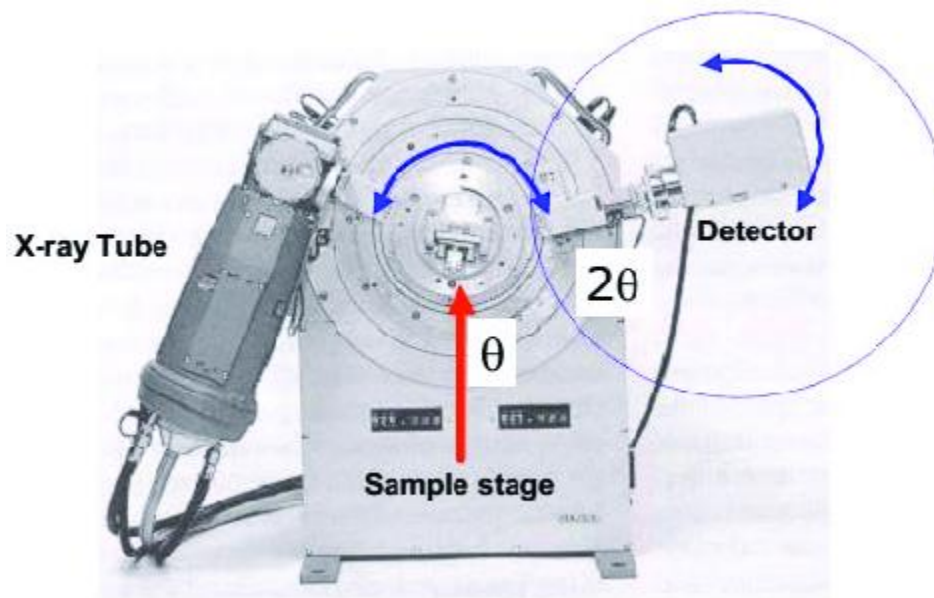


Figure 3.6 Fundamental parts of a X-ray diffractometer [43]

### **3.3.3 Scanning Electron Microscope (SEM)**

Scanning electron microscopy (SEM) is an imaging method which employs a focused electron beam to get high-resolution images of solid samples. In addition to imaging, SEM can also be used for elemental analysis of the sample. The most commonly used imaging mode in SEM is the secondary electron image, which provides a map of secondary electron emissions as a function of spatial position. The topography of the sample may be visualised by using this emission intensity, which depends on the angle between the surface and the beam. Figure 3.7 shows an example of a secondary electron image obtained using SEM.

**Working Principle:** When primary electrons are directed towards the sample in SEM, they generate secondary electrons of less energy. The detection and mapping of these secondary electrons provide information about the topography of the specimen.

#### **3.3.3.1 SEM Instrumentation**

The electron optical system is utilized as the primary means for generating a probe electron beam, which involves the use of an electron gun, condenser lens, objective lens, and scanning coil. The electron gun serves as the source for producing the electron beam, while the lenses are responsible for focusing and adjusting the diameter of the beam. Additionally, a specimen stage is incorporated into the system for holding the specimen being analyzed, and a secondary electron detector is employed for collecting secondary electrons emitted from the specimen. The resulting data is then transformed into an image format and displayed on a display unit that is connected to an operating system, which allows for various operations to be carried out.



This method is especially helpful in determining the band-gap of semiconducting materials. A UV-Vis spectrometer is commonly employed for this purpose, and its experimental set-up typically involves a sample compartment where the sample is placed, a light source that emits light in the UV-Vis range, a monochromator for selecting a specific wavelength of light, a cuvette for containing sample, along with a detector for measuring intensity of transmitted light. This band-gap of material that is semiconducting could be determined utilizing the data from this experiment. Figure depicts the UV-Vis spectrometer experimentation setup:

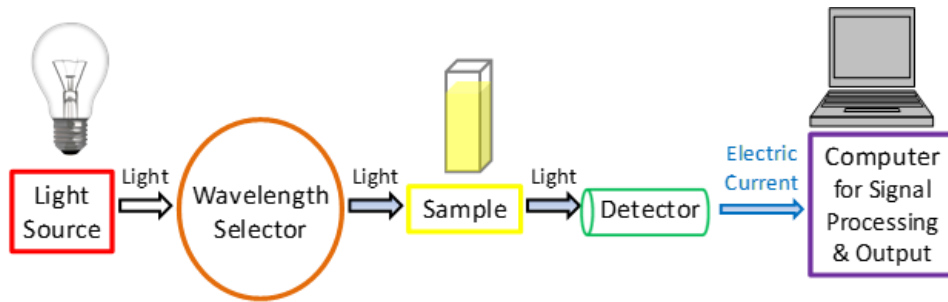


Figure 3.8. The experimental design of UV-Vis spectrometer [44].

The process of synthesizing materials has been successfully established and has undergone comprehensive discussion in terms of the synthesis process of the photoanode, counter electrode, dye material, and electrolyte. Furthermore, fundamental characterization techniques have been introduced.

## Chapter 4

### Results and Discussion

The current chapter will outline the findings as well as evaluating the TiO<sub>2</sub> nanorod arrays that were synthesized on FTO substrates at varying reaction times using a variety of characterization methods, including field-emission scanning electron microscopy (FE-SEM), X-ray diffraction (XRD), Raman spectroscopy as well as UV-Vis spectroscopy. Additionally, the resulting structures efficiency will be assessed using a solar cell simulator.

#### 4.1 Investigation of TiO<sub>2</sub> layer

##### 4.1.1 XRD analyses of TiO<sub>2</sub> layer

Figure 4.1 presents the X-ray diffraction (XRD) pattern of vertically aligned TiO<sub>2</sub> nanorods (TNRs) on a *c*-TiO<sub>2</sub> coated FTO substrate. The XRD analysis confirms that the TiO<sub>2</sub> NRs film is primarily composed of tetragonal rutile phase, corresponding to the ICSD No. 1511015, with 1-D TNRs crystallized tetragonally and belonging to the P 4<sub>2</sub>/m n m space group. Characteristic XRD peaks are observed at 2θ angles of 26.248°, 27.238°, 35.879°, 37.539°, 41.055°, 54.275°, and 62.647°, corresponding to the (110), (121), (101), (200), (111), (211), and (002) planes, respectively. Additionally, an asterisk (\*) is used to indicate the FTO peaks, which are also seen in the TNRs film's XRD pattern as well. The intensity of the (110) and (200) planes is notably higher than that of the other planes, which can be attributed to the preferential growth direction of the TNRs. The slight lattice mismatch between FTO and TNRs may have contributed to the production of the rutile phase through hydrothermal synthesis, rather than other phases such as anatase or brookite.

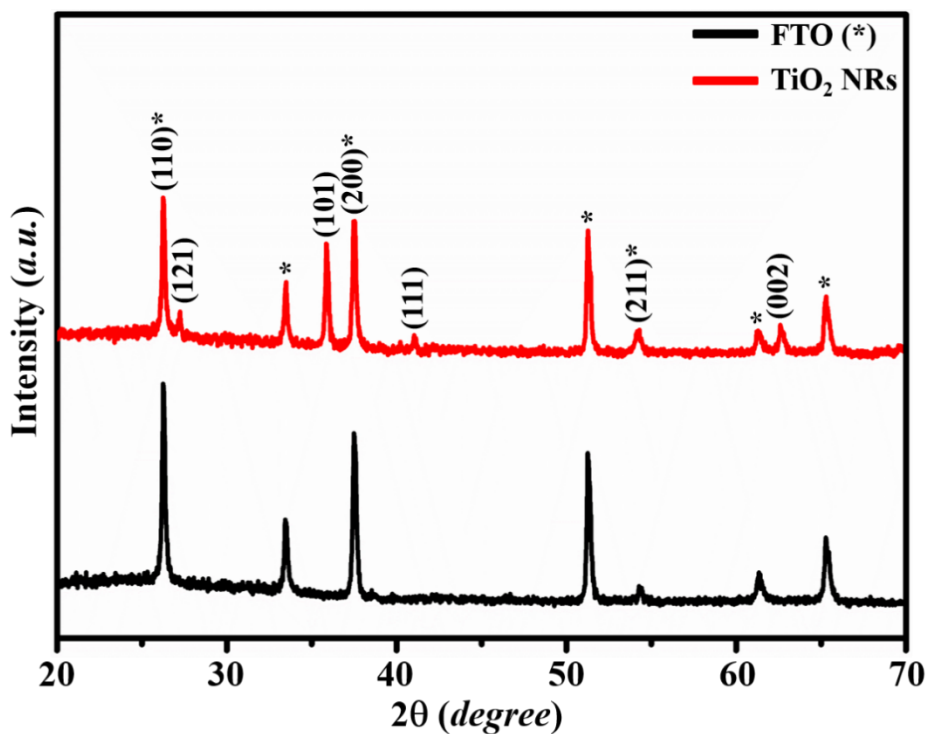


Figure 4.1 shows a pattern of X-ray diffraction (XRD) and corresponding peaks of TiO<sub>2</sub> nanorod (NR) photoanodes fabricated on *c*-TiO<sub>2</sub> layer coated FTO substrates.

Rutile phase TiO<sub>2</sub> nanorods (TNRs) and SnO<sub>2</sub> have almost identical lattice parameters, allowing for the epitaxial growth of rutile TiO<sub>2</sub> on FTO film. Specifically, TiO<sub>2</sub> has lattice parameters of  $a=4.594\text{\AA}$ , along with  $c=2.958\text{\AA}$ , while SnO<sub>2</sub> has lattice parameters of  $a=4.737\text{\AA}$ , along with  $c=3.185\text{\AA}$ . In this investigation, the Xpert-High-score fitted values of rutile phase TNRs were  $a=4.609\text{\AA}$  and  $c=2.968\text{\AA}$ , while the estimated lattice constants were  $a=4.612\text{\AA}$  and  $c=2.967\text{\AA}$ , with very little variation of  $\pm 0.003\text{\AA}$  and  $\pm 0.001\text{\AA}$ , respectively. On the other hand, anatase and brookite phases of TNRs have lattice constants of  $a=3.784\text{\AA}$ ,  $c=9.514\text{\AA}$ , along with  $a=5.455\text{\AA}$ ,  $c=5.142\text{\AA}$ , respectively. These phases were not observed in this study, likely due to the high activation energy threshold required for their production, which cannot be achieved at the relatively low temperatures used in this hydrothermal reaction. [45]

#### 4.1.2 FE-SEM Analyses of TiO<sub>2</sub> Nanorods

The FESEM images of the produced TNR photoanodes are presented in Figure 4.2. The images depict that the rods resemble seagrass in shape. The TNRs exhibit a uniform and vertically decorated configuration at different magnifications, as depicted in Figure 4(a, b). It was found that TNRs tend to form clumps when they are gathered collectively. The inset of Figure 4(a) shows the average length and width of TNRs organized in clumps. The cross-sectional FESEM image indicates that the TNRs have a length ranging from 1.106-1.452  $\mu\text{m}$  and a breadth ranging from 80-95 nm. The shape and crystallinity of the TNR photoanodes produced are strongly influenced by the HCl content. The shape and the crystalline phase of TiO<sub>2</sub> nanostructures are closely related. HCl is necessary for the hydrothermal production of seagrass-like rutile TNR arrays because of strong water reactivity of starting materials of titanium. It is employed to regulate the hydrolysis and nucleation rate during the TNR synthesis process.

Glacial acetic acid is utilized as a stabilizing agent to avert hydrolysis during the synthesis of titanium oxide (TiO<sub>2</sub>) nanorods. The strong affinity of Ti<sup>4+</sup> with water necessitates prior stabilization to avoid hydrolysis. Therefore, glacial acetic acid is used as a stabilizing agent and catalyst during the production of Ti(OBu)<sub>4</sub>. By condensation, acetic acid stabilizes Ti(OBu)<sub>4</sub>, resulting in the formation of continuous chains with high surface area. The combination of glacial acetic acid and Ti(OBu)<sub>4</sub> initiates the chemical reaction, and selective, seagrass-like, one-dimensional TiO<sub>2</sub> nanorods begin to grow on the substrate surfaces. The nanorods are arranged in a pattern facing away from the FTO surface, indicating that adding acetic acid to the HCl solution improves the development of better-coordinated, vertically aligned nanorods on the FTO substrate. The existence of Ti and O without any foreign species is confirmed through EDS and elemental mapping spectra, which are uniformly distributed throughout the surface, resulting in highly stable structural, morphological, as well as chemical properties of synthesized TiO<sub>2</sub>

nanorods. This obtained results are consistent with the literature available. [46]

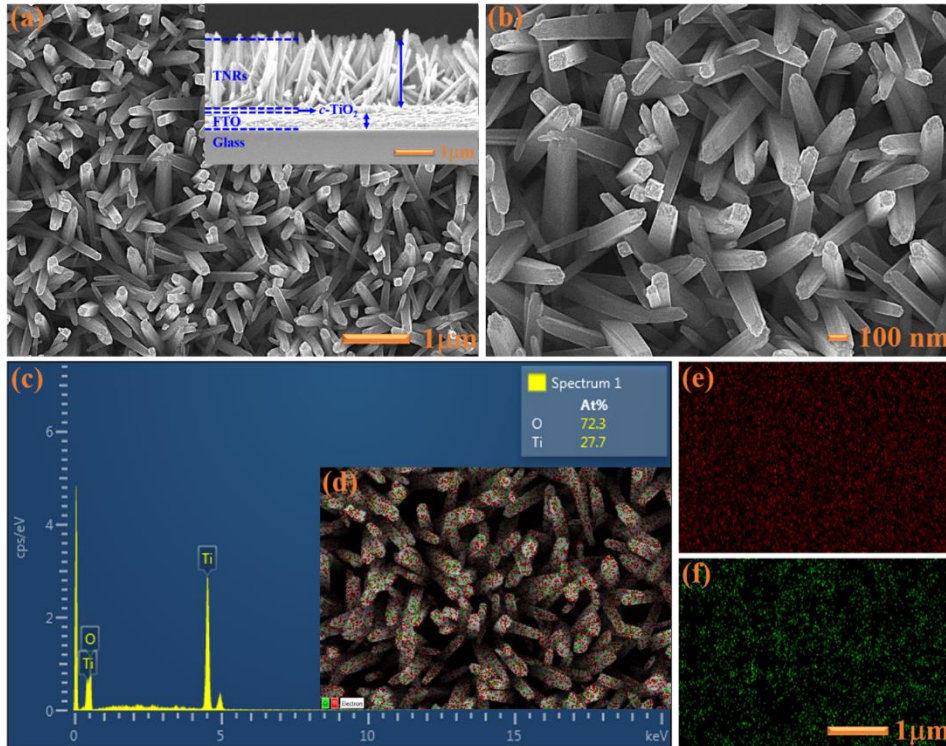


**Figure 4.2** Typical surface morphology and compositional analysis. (a-b) high-resolution FESEM images, (c) EDS analysis, (d) electron image for elemental mapping, (e) Ti-distribution, and (f) O-distribution.

#### 4.1.3 UV-Vis spectroscopy analyses of TiO<sub>2</sub> Nanorods

The optical characteristics of TiO<sub>2</sub> nanorods (TNRs) were examined utilizing UV-visible absorption spectroscopy. The absorption spectra of TNRs were recorded, as well as Tauc's plot was used to find the bandgap energy. A sharp absorption peak was observed at approximately 340 nm, which was used to calculate the size of the rutile TNRs. Since the size of TNRs is much larger than the Bohr exciton diameter

of TiO<sub>2</sub>, no observable blue shift caused by quantum confinement was observed. The high degree of photo scattering from TNRs resulted in low absorption (10-20%) in the wavelength range of 350-500 nm. These findings had been presented in Figure 4(a), with the corresponding Tauc's plot depicted in Figure 4(b).

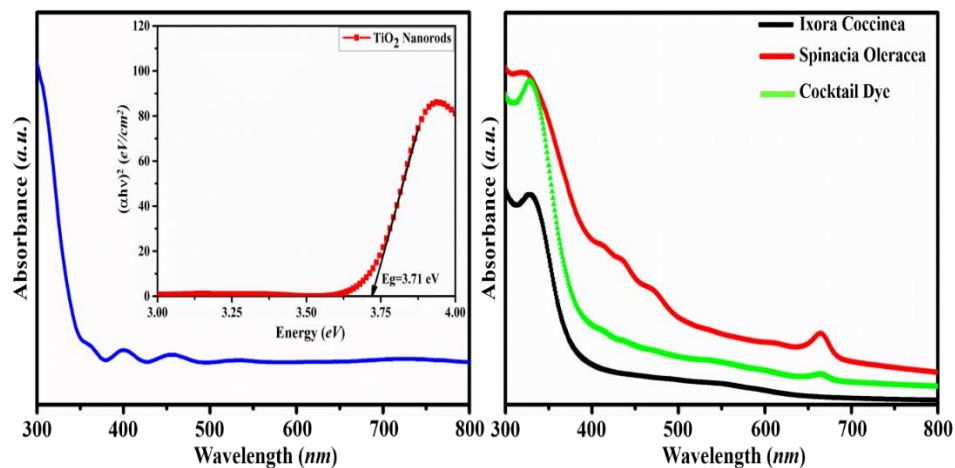


**Figure 4.3** UV-visible spectroscopy analysis. (a) Absorption spectra of hydrothermally synthesized TNRs, (b) Bandgap estimation of the respective TNRs, (c) Absorption spectra of SOL<sub>(red)</sub>, ICF<sub>(black)</sub>, and cocktail<sub>(green)</sub> dyes.

The bandgap ( $E_g$ ) of the synthesized TNRs was determined to be 3.71 eV, as illustrated in Figure 4(b), which is in accordance to theoretical value of 3.2 eV. It indicates that TNR photoanodes effectively absorb UV-light and transmit the entire visible spectrum for dye excitation. The capability of dyes to absorb light and their influence on the creation and transfer of photo charges in emerging devices had been investigated using UV-Visible spectroscopy. This absorption spectrum of ICF exhibits broad absorption from  $\lambda=400$  to 700 nm with two maximum absorption peaks at  $\lambda=550$  and 660 nm. Chlorophylls exhibit absorption at both lower and higher wavelengths, with four principal absorption peaks at  $\lambda=668$ , 472, 441, and 413 nm. The peaks at 413 and 668 nm were identified as characteristic peaks of chlorophyll-a, while the other two peaks observed in between correspond to carotenoid characteristic peaks. Co-sensitized dyes in the volume ratio of (1:1 v:v)

exhibited absorption throughout the visible region, consisting of characteristic absorption peaks at 668, 540, and 410-435 nm. These optical absorption experimental analyses are in agreement with current literature and demonstrate the promising potential of natural dyes for highly efficient and stable DSSC applications [47][48].

#### **4.1.4 Raman spectroscopy**

To validate the formation of TNRs and to analyse the phase composition of the TNR photoanodes, Raman spectroscopy was used. The rutile phase of TNRs belongs to the tetragonal space group  $P4_2/mnm$ , with lattice parameters  $a=b$ , along with  $c$ . The lattice structure of rutile consists of two  $TiO_2$  units, where  $Ti^{4+}$  atoms are located at  $(0, 0, 0)$  and  $(\frac{1}{2}, \frac{1}{2}, \frac{1}{2})$ , and  $O^{2-}$  atoms occupy positions  $\pm(u, u, 0)$  and  $\pm(\frac{1}{2}+u, \frac{1}{2}-u, \frac{1}{2})$ . The rutile crystal structure has 5 Raman active modes, namely:  $B1g$ , multi-phonon process,  $Eg$ ,  $A1g$ , along with  $B2g$ . These characteristic Raman active modes of rutile phase TNRs, including  $B1g$ ,  $Eg$ ,  $A1g$ , and  $B2g$ , were observed at 144.4, 446.7, 609.8, and 707.2  $cm^{-1}$ , accordingly, as depicted in Figure 4.8

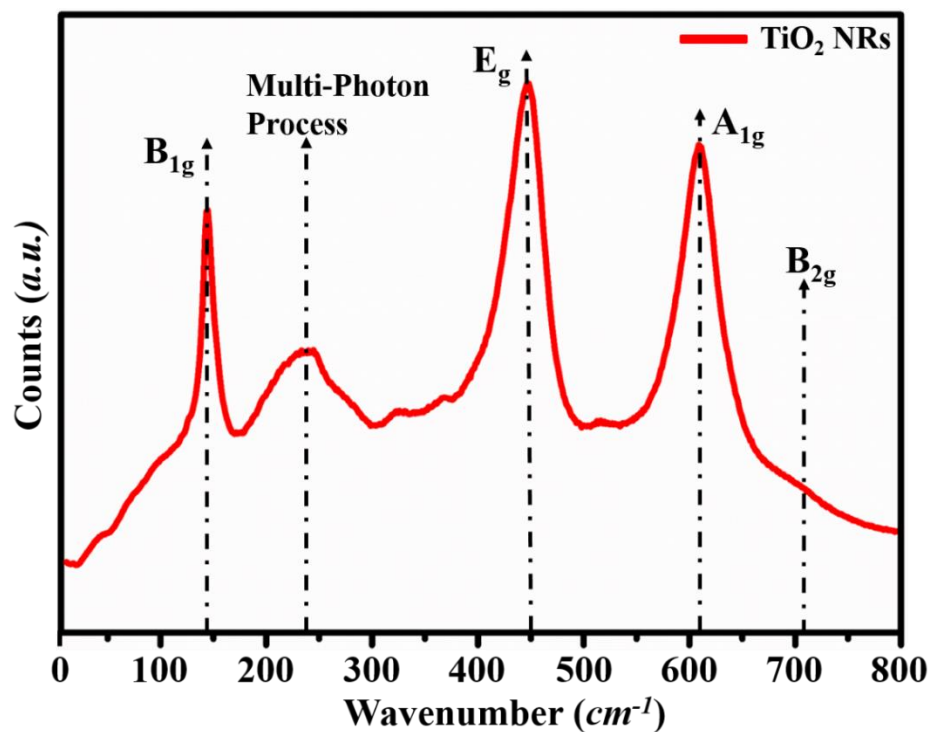


**Figure 4.4.** Raman spectra of the hydrothermally synthesized TNRs on the *c*-TiO<sub>2</sub> coated FTO substrates, which were used as a photoanode in DSSC application.

In addition, an extra peak at 240.9 cm<sup>-1</sup> had been noticed, attributed to multi-photon process. The B<sub>1g</sub> and E<sub>g</sub> peaks are indicative of symmetric O-Ti-O bending and stretching vibrations, respectively, while the A<sub>1g</sub> peak is another dominant vibrational peak. The intense and wide peak at 240.9 cm<sup>-1</sup> is related to multi-photon process, which arises due to photon scattering and is consistent with previous literature. This finding supports the XRD result that TNRs are predominantly composed of rutile phase. The bending, stretching, and vibrations of atoms and molecules change as the dimensions of the bulk phase are lowered to the nanoscale or smaller, known as phonon confinement, which manifests as blue-shifts and red-shifts in the Raman bands. The slight variation in the experimental findings from previous reports is attributed to induced lattice strains during thermal annealing. The Raman analysis concludes that annealing improves the crystallinity quality of the

TNRs, with no significant effect on grain size and faceting, further confirming the presence of rutile crystalline phases. [49]

#### 4.1.5 I-V Characteristics of solar cell

The synthesized dye-sensitized solar cells (DSSCs) using natural dyes, such as SOL, ICF, and a cocktail of these two dyes, were characterized using photocurrent-voltage (J-V) analysis. The DSSCs were constructed with three different counter electrodes, Carbon (C), Ni<sub>Pressed</sub> (Ni<sub>P</sub>), and Ni<sub>non-Pressed</sub> (Ni<sub>nP</sub>), and tested under standard solar irradiance using a solar simulator. The devices were structured as FTO/c-TiO<sub>2</sub>/TNRs/Dyes/Electrolyte/C. The photovoltaic performance of SOL and ICF dye-based DSSCs was shown in Figure 4.9(a) and (c), while the cocktail dye-based DSSC was shown in Figure 4.9(b).

The maximum power conversion efficiencies( $\eta$ ) for SOL, ICF, and cocktail dye-based DSSCs were 1.04%, 0.57%, and 2.39%, respectively, with the carbon-based counter electrode. The current-density ( $J_{SC}$ ), open-circuit voltage ( $V_{OC}$ ), Fill-factor (FF), and efficiency ( $\eta$ ) for other counter electrode-based DSSCs were summarized in Table 1. The FTO/c-TiO<sub>2</sub>/TNRs/Dyes/Electrolyte/C structured DSSCs sensitized with cocktail, SOL, and ICF dyes showed maximum  $J_{SC}$  values of 2050, 1297, and 625  $\mu A/cm^2$ , respectively, which agreed well with the photovoltaic performance results. The high  $J_{SC}$  values were attributed to the strong dye loading/binding on the TNRs surface and effective electron-diffusion in DSSC assembly. DSSCs with Ni<sub>nP</sub> and Ni<sub>P</sub> counter electrodes exhibited lower  $J_{SC}$  values compared to those with C-based counter electrodes.

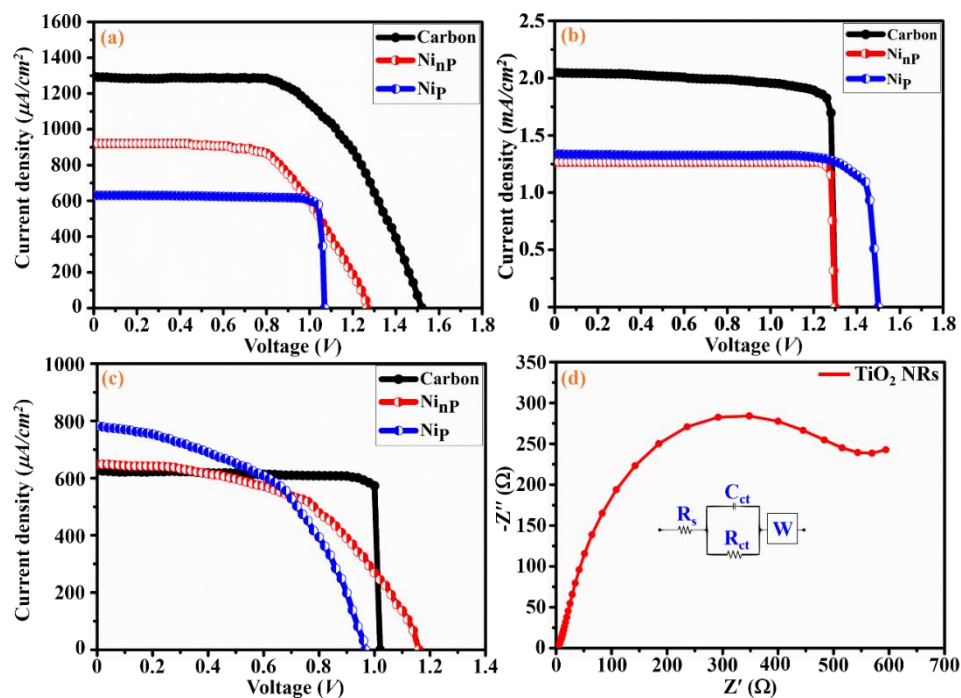


**Figure 4.5.** Photovoltaic analysis of the prepared DSSCs utilizing natural SOL, ICF, cocktail dyes and C/Ni<sub>NP</sub>/Ni<sub>P</sub> counter electrodes. (a) FTO/c-TiO<sub>2</sub>/TNRs/SOL/Electrolyte/(C/Ni<sub>NP</sub>/Ni<sub>P</sub>), (b) FTO/cTiO<sub>2</sub>/TNRs/Cocktail/Electrolyte/(C/Ni<sub>NP</sub>/Ni<sub>P</sub>), (c) FTO/c-TiO<sub>2</sub>/TNRs/ICF/Electrolyte/(C/Ni<sub>NP</sub>/Ni<sub>P</sub>), and (d) electrochemical impedance spectra (EIS).

<i>Dyes</i>	<i>Device structure</i>	<i>J<sub>sc</sub></i> ( $\mu\text{A}/\text{cm}^2$ )	<i>V<sub>oc</sub></i> (V)	<i>FF</i>	<i><math>\eta</math></i> (%)
<i>Cocktail</i>	FTO/c-TiO <sub>2</sub> /TNRs/Dye/Electrolyte/C	2050	1.300	0.89	2.39
<i>l</i>	FTO/c-TiO <sub>2</sub> /TNRs/Dye/Electrolyte/Ni <sub>NP</sub>	1268	1.300	0.98	1.62

<b>(1:1</b>	FTO/c-	1339	1.500	0.78	1.58
<b>v:v)</b>	TiO <sub>2</sub> /TNRs/Dye/Electrolyte/Ni <sub>P</sub>				
<b>SOL</b>	FTO/c-TiO <sub>2</sub> /TNRs/Dye/Electrolyte/C	1297	1.520	0.52	1.04
<b>Dye</b>	FTO/c-	920	1.265	0.59	0.70
	TiO <sub>2</sub> /TNRs/Dye/Electrolyte/Ni <sub>NP</sub>				
	FTO/c-	630	1.069	0.95	0.64
	TiO <sub>2</sub> /TNRs/Dye/Electrolyte/Ni <sub>P</sub>				
<b>ICF</b>	FTO/c-TiO <sub>2</sub> /TNRs/Dye/Electrolyte/C	625	1.020	0.90	0.57
<b>Dye</b>	FTO/c-	649	1.160	0.52	0.39
	TiO <sub>2</sub> /TNRs/Dye/Electrolyte/Ni <sub>NP</sub>				
	FTO/c-	782	0.967	0.50	0.38
	TiO <sub>2</sub> /TNRs/Dye/Electrolyte/Ni <sub>P</sub>				

---

The objective of this investigation was to design and characterize titanium nanorods (TNRs) for efficient light absorption and charge separation, in addition to developing cocktail-based dye-sensitized solar cells (DSSCs) towards applications in photovoltaics. The impact of cocktail dyes on DSSCs was systematically investigated. Co-sensitized TNRs-based DSSCs showed improved performance parameters, including power conversion efficiency ( $\eta$ ), current density ( $J_{SC}$ ), open-circuit voltage ( $V_{OC}$ ), as well as fill factor (FF). Investigations were also conducted on the usage of natural sensitizers in the the process of extraction, fabrication, and DSSCs photovoltaic performance. Natural dyes were extracted using simple methods, and their UV-visible spectroscopy was analyzed. Chlorophyll showed the highest efficiency and lifetime among the extracted dyes. The DSSCs fabricated by employing cocktail dyes demonstrated the greater effectiveness, having a power conversion efficiency ( $\eta$ ) of 2.39%.

## Chapter 5

### Conclusions and Future Potential

The purpose of the present research project intends that of creating a dye-sensitized solar cell (DSSC) and improve its performance by using natural dyes that have been derived from the flowers and leaves of *Spinacia oleracea* and *Ixora coccinea*, respectively. The materials used in DSSCs are cost-effective, environmentally friendly, and are readily available. After the TiO<sub>2</sub> photoelectrode was annealed at various temperatures, nanorods were created on the fluorine-doped tin oxide substrate covered in a compact layer. While the diameter of the nanorods was affected by the precursor concentration, the length was found to vary with reaction time. The structural, optical, and morphological characteristics of the nanorods had been analyzed employing X-ray diffraction (XRD), UV-Visible spectroscopy, along with field emission scanning electron microscopy, respectively. XRD confirmed the presence of rutile TiO<sub>2</sub> nanostructures, while UV-Vis spectroscopy determined the bandgap to be 3.71 eV. The electrolyte was prepared by oxidizing iodide in the absence of sunlight, and the natural dye from *Ixora Coccinea* and Spinach was characterized using UV-Visible spectroscopy to understand its absorbance. Using nickel or carbon as the counter electrode with a combination of potassium iodide, iodine crystal, along with ethylene glycol as the electrolyte boosted DSSC's efficiency. The maximum energy conversion efficiency achieved had been 2.39%, as measured using a solar simulator.

### Future Scope

There is much work to be done on DSSC

1. Enhancement in efficiency
2. Only  $I/I_3^-$  redox couple has slow recombination kinetics
3. It is difficult to handle liquid electrolyte because it contracts at lower temperatures and expands at higher temperatures, instead use solid electrolyte to overcome this.

4. More doors should be opened in future to explore the practical applications of DSSC.
5. Oxidation migration affects the stability concerning dye-sensitized solar cells over every course associated with their lifetime. In future the work will be carried out to address these issues

## References

- [1] (2015-2016) Energy from the Sun, Student Guide. National Energy Education Development Project (NEED).
- [2] IRENA (2019c), Renewable capacity statistics 2019, International Renewable Energy Agency, Abu Dhabi.
- [3] G. Richhariya, A. Kumar, P. Tekasakul, B. Gupta, Natural dyes for dye sensitized solar cell: A review, *Renew. Sustain. Energy Rev.* 69 (2017) 705–718. <https://doi.org/10.1016/j.rser.2016.11.198>.
- [4] Yadav, A. and Kumar, P. (2015) Enhancement in Efficiency of PV Cell through P&O Algorithm. *International Journal for Technological Research in Engineering*, 2, 2642-2644.
- [5] G. Richhariya, A. Kumar, P. Tekasakul, B. Gupta, Natural dyes for dye sensitized solar cell: A review, *Renew. Sustain. Energy Rev.* 69 (2017) 705–718. <https://doi.org/10.1016/j.rser.2016.11.198>.
- [6] McEvoy, A., Castaner, L. and Markvart, T. (2012) *Solar Cells: Materials, Manufacture and Operation*. 2nd Edition, Elsevier Ltd., Oxford, 3-25.
- [7] Najm AS, Mohamad AB, Ludin NA. The extraction and absorption study of natural dye from Areca catechu for dye sensitized solar cell application. *Am Inst Phys.* 2017;20019:020019
- [8] Ludin NA, Mahmoud AMA, Bakar A. Review on the development of natural dye photosensitizer for dye-sensitized solar cells. *Renew Sustain Energy Rev.* 2014;31(March):386-396.

- [9] Choubey, P.C., Oudhia, A. and Dewangan, R. (2012) A Review: Solar Cell Current Scenario and Future Trends. *Recent Research in Science and Technology*, 4, 99-101
- [10] Bertolli, M. (2008) Solar Cell Materials. Course: Solid State II. Department of Physics, University of Tennessee, Knoxville.
- [11] Jayakumar, P. (2009) Solar Energy Resource Assessment Handbook. Renewable Energy Corporation Network for the Asia Pacific
- [12] Chopra, K.L., Paulson, P.D. and Dutt, V. (2004) Thin-Film Solar Cells: An Overview. *Progress in Photovoltaics*, 12, 69-92.  
<http://dx.doi.org/10.1002/pip.541>
- [13] Maehlum, M.A. (2015) Energy Informative The Homeowner's Guide To Solar Panels, Best Thin Film Solar Panels— Amorphous, Cadmium Telluride or CIGS? Last updated 6 April 2015.
- [14] Elsabay, K.M., El-Hawary, W.F. and Refat, M.S. (2012) Advanced Synthesis of Titanium-Doped-Tellurium-Cadmium Mixtures for High Performance Solar Cell Applications as One of Renewable Source of Energy. *International Journal of Chemical Sciences*, 10, 1869-1879.
- [15] Badawy, W.A. (2015) A Review on Solar Cells from Si-Single Crystals to Porous Materials and Quantum Dots. *Journal of Advanced Research*, 6, 123-132. <http://dx.doi.org/10.1016/j.jare.2013.10.00>
- [16] Srinivas, B., Balaji, S., Nagendra Babu, M. and Reddy, Y.S. (2015) Review on Present and Advance Materials for Solar Cells. *International Journal of Engineering Research-Online*, 3, 178-182.
- [17] Gokilamani, N., et al. "Utilization of natural anthocyanin pigments as photosensitizers for dye-sensitized solar cells." *Journal of sol-gel science and technology* 66 (2013): 212-219.

- [18] Al-Bat'hi, Souad Ali, Iraj Alaei, and Iis Sopyan. "Natural photosensitizers for dye sensitized solar cells." *International Journal of Renewable Energy Research* 3.1 (2013): 138-143.
- [19] Maiaugree, Wasan, et al. "A dye sensitized solar cell using natural counter electrode and natural dye derived from mangosteen peel waste." *Scientific reports* 5.1 (2015): 1-12.
- [20] Yu H, Zhang S, Zhao H, Xue B, Liu P, Will G. High-performance TiO<sub>2</sub> photoanode with an efficient electron transport network for dye-sensitized solar cells. *J Phys Chem C* 2009;113:16277–82.
- [21] Francis, O. and Ikenna, A. (2021) Review of Dye-Sensitized Solar Cell (DSSCs) Development. *Natural Science*, **13**, 496-509.
- [22] Costas Prouskas 1,\* , Angelos Mourkas 1 , Georgios Zois 1 , Elefterios Lidorikis 1,2 and Panos Patsalas , A New Type of Architecture of Dye-Sensitized Solar Cells as an Alternative Pathway to Outdoor Photovoltaics, *Energies* 2022, 15, 2486
- [23] Mohiuddin, O., Obaidullah, M. & Sabah, C. Improvement in dye sensitized solar cells from past to present. *Opt Quant Electron* **50**, 377 (2018).
- [24] Jaafar, Hidayani, Mohd Fadzil Ain, and Zainal Arifin Ahmad. "Performance of *E. conferta* and *G. atroviridis* fruit extracts as sensitizers in dye-sensitized solar cells (DSSCs)." *Ionics* 24 (2018): 891-899.
- [25] Narayan, M., and A. Raturi. "Investigation of some common Fijian flower dyes as photosensitizers for dye sensitized solar cells abstract." *Applied Solar Energy* 47 (2011): 112-117.

- [26] Hosseinnezhad, Mozhgan, Siamak Moradian, and Kamaladin Gharanjig. "Fruit extract dyes as photosensitizers in solar cells." *Current Science* (2015): 953-956.
- [27] J. H. Rhee, C-C. Chung and E. W-G. Diau, *NPG Asia Materials*, 2013, 5, e68.
- [28] O.O. Nnorom, G.C. Onuegbu, C.K.A. Joe-Uzuegbu, E.E. Atimati, Natural Dye Sensitized Solar Cell Conversion Efficiency Enhancement: A Review, 2020 IEEE PES/IAS PowerAfrica, PowerAfrica 2020. (2020) 1–6.
- [29] Karki, Indra B., et al. "Dye-sensitized solar cells sensitized with natural dye extracted from Indian Jamun." *Bibechana* 11 (2014): 34-39.
- [30] Ossai, Amarachukwu N., et al. "Zinc oxide-based dye-sensitized solar cells using natural and synthetic sensitizers." *Current Research in Green and Sustainable Chemistry* 3 (2020): 100043.
- [31] S.C. Yadav, A. Sharma, R.S. Devan, P.M. Shirage, Role of different counter electrodes on performance of TiO<sub>2</sub> based dye-sensitized solar cell (DSSC) fabricated with dye extracted from Hibiscus Sabdariffa as sensitizer, *Opt. Mater. (Amst)*. 124 (2022).  
<https://doi.org/10.1016/j.optmat.2022.112066>.
- [32] P. Cheng, Y. Liu, P. Sun, S. Du, Y. Cai, F. Liu, J. Zheng, G. Lu, Hydrothermally growth of novel hierarchical structures titanium dioxide for high efficiency dye-sensitized solar cells, *J. Power Sources*. 268 (2014) 19–24.
- [33] M. D. Tyona, "A theoretical study on spin coating technique," *Adv. Mater. Res.*, vol. 2, no. 4, pp. 195–208, 2013,  
doi: 10.12989/amr.2013.2.4.195.
- [34] B. S. Yilbas, A. Al-Sharafi, and H. Ali, *Surfaces for Self-Cleaning*. 2019.

- [35] Richhariya, Geetam, et al. "Natural dyes for dye sensitized solar cell: A review." *Renewable and Sustainable Energy Reviews* 69 (2017): 705-718.
- [36] Garima Dwivedi , Guncha Munjal , Ashok N. Bhaskarwar , Amita Chaudhary, Dye-sensitized solar cells with polyaniline: A review, *Inorganic Chemistry Communications* 135 (2022) 109087.
- [37] M. D. Tyona, "A theoretical study on spin coating technique," *Adv. Mater. Res.*, vol. 2, no. 4, pp. 195–208, 2013,
- [38] "Chapter 2 Experimental techniques: Hydrothermal synthesis and characterization tools," pp. 39–68.
- [39] S.C. Yadav, A. Sharma, R.S. Devan, P.M. Shirage, Role of different counter electrodes on performance of TiO<sub>2</sub> based dye-sensitized solar cell (DSSC) fabricated with dye extracted from Hibiscus Sabdariffa as sensitizer, *Opt. Mater. (Amst)*. 124 (2022).
- [40] A. Srivastava, B. Singh Chauhan, S. Chand Yadav, M. Kumar Tiwari, J. Akash Kumar Satrughna, A. Kanwade, K. Bala, P.M. Shirage, Performance of dye-sensitized solar cells by utilizing Codiaeum Variegatum Leaf and Delonix Regia Flower as natural sensitizers, *Chem. Phys. Lett.* 807 (2022) 140087.
- [41] A. Srivastava, B. Singh Chauhan, S. Chand Yadav, M. Kumar Tiwari, J. Akash Kumar Satrughna, A. Kanwade, K. Bala, P.M. Shirage, Performance of dye-sensitized solar cells by utilizing Codiaeum Variegatum Leaf and

- Delonix Regia Flower as natural sensitizers, *Chem. Phys. Lett.* 807 (2022) 140087.
- [42] S. Eiden-Assmann and G. Maret, "CeF<sub>3</sub> nanoparticles: Synthesis and characterization," *Mater. Res. Bull.*, vol. 39, no. 1, pp. 21–24, 2004,
- [43] Suastika, Komang Gde, et al. "Characterization of central Kalimantan's amethysts by using x-ray diffraction." *Journal of Physics: Conference series*. Vol. 846. No. 1. IOP Publishing, 2017.
- [44] Tom, Justin. "UV-Vis Spectroscopy: Principle, Strengths and Limitations and Applications Article Published: June 30, 2021."
- [45] W.K. Wang, J.J. Chen, X. Zhang, Y.X. Huang, W.W. Li, H.Q. Yu, Self-induced synthesis of phase-junction TiO<sub>2</sub> with a tailored rutile to anatase ratio below phase transition temperature, *Sci. Rep.* 6 (2016) 1–10.
- [46] S.S. Mali, H. Kim, C.S. Shim, P.S. Patil, J.H. Kim, C.K. Hong, Surfactant free most probable TiO<sub>2</sub> nanostructures via hydrothermal and its dye sensitized solar cell properties, *Sci. Rep.* 3 (2013) 1–8.
- [47] N.T.R.N. Kumara, P. Ekanayake, A. Lim, L.Y.C. Liew, M. Iskandar, L.C. Ming, G.K.R. Senadeera, Layered co-sensitization for enhancement of conversion efficiency of natural dye sensitized solar cells, *J. Alloys Compd.* 581 (2013) 186–191.
- [48] D. Sengupta, B. Mondal, K. Mukherjee, Visible light absorption and photo-sensitizing properties of spinach leaves and beetroot extracted natural dyes,

Spectrochim. Acta - Part A Mol. Biomol. Spectrosc. 148 (2015) 85–92.

- [49] C.M. Mbulanga, R.M. Erasmus, Z.N. Urgessa, S.R.T. Djiokap, E.J. Olivier, W.E. Goosen, J.R. Botha, R. Betz, Raman spectroscopy characterisation of oriented bundles of single-crystal rutile-phase TiO<sub>2</sub> nanorods prepared by hydrothermal bath deposition on transparent conducting substrates, *Appl. Phys. A Mater. Sci. Process.* 125 (2019) 1–10.
- [50] Teja, Akula Surya, et al. "Optimal processing methodology for futuristic natural dye sensitized solar cells and novel applications." *Dyes and Pigments* (2022): 110997.